THEORETICAL STUDIES OF PHOTOSYNTHESIS

By
MARK ALAN THOMPSON

A DISSERTATION PRESENTED TO THE GRADUATE SCHOOL
OF THE UNIVERSITY OF FLORIDA IN PARTIAL FULFILLMENT
OF THE REQUIREMENTS FOR THE DEGREE OF
DOCTOR OF PHILOSOPHY

UNIVERSITY OF FLORIDA

1990

ACKNOWLEDGMENTS

I was fortunate to have started graduate school at the beginning of a very exciting period in chemistry. Breakthroughs in understanding the atomic structure of bacterial photosynthetic reaction centers had just been announced. These advancements created great opportunities in theoretical chemistry for studying photosynthetic electron transfer, arguably the most important series of chemical transformations for life on this planet. Everywhere I looked there were interesting and totally new aspects of this area to study. I am grateful for this unique opportunity. I would like to acknowledge Professor Michael Zerner and Dr. Jack Fajer for making this possible for me.

Life as a graduate student can be an ascetic, albeit intellectually stimulating, period in one's life. To survive these last few years has required a high level of dedication and commitment to research. This commitment, however, pales in comparison to that of my wife Vivienne. Her unfailing love and patience and her ability to keep my feet on the ground have been crucial to my finishing this degree. It is to Vivienne that I dedicate this dissertation.

I would like to welcome my brand new son Douglas to the world. I hope he finds it as interesting and fun as I do.

TABLE OF CONTENTS

Abstract of Dissertation Presented to the Graduate School
of the University of Florida in Partial Fulfillment of the
Requirements for the Degree of Doctor of Philosophy

THEORETICAL STUDIES OF PHOTOSYNTHESIS

By

MARK ALAN THOMPSON

August 1990

Chairman: Professor Michael C. Zerner
Major Department: Chemistry

The conversion of light energy to chemical energy by the process of photosynthetic charge separation is one of the most important chemical transformation for life on this planet. With the atomic level structures of photosynthetic reaction centers (RC) for some bacteria now known, we can attempt to attain a more complete understanding of the properties and mechanisms of these systems. In this dissertation theoretical studies on both monomeric bacteriochlorophylls (BChl) and aggregates of these and related pigments representing models of the RC are presented. Models for the effects of nearby charged and polar groups on monomeric BChls and how these relate to spectroscopic shifts in the absorption spectrum of the RC are discussed. The calculated properties of the BChl dimer or "special pair" is best described in terms of a dimer of strongly interacting BChl monomers rather than the more traditional coupled chromophore model. That this BChl dimer is responsible for the lowest absorption band in the UV/vis spectrum of RCs is well described by these results. A description of these interactions in the BChl dimer

is presented using a simpler model system composed of Mg-bacteriochlorin dimers. A model of the RC consisting of the four BChlbs and two bacteriopheophytins as well as some of the surrounding amino acids of the RC protein is sufficient to give a reasonable description of the calculated UV/vis spectrum of the RC. These results show that the lowest two excited states of the RC are attributed to the BChl dimer. This strengthens the identification of the second lowest excited state with the shoulder seen at 850 nm in experimental spectra as the upper exciton-like component of the BChl dimer. Charge transfer (CT) states are calculated and demonstrate the preference for flow of charge in the RC along only one of its branches.

CHAPTER 1
INTRODUCTION

Historical

The history of research in photosynthesis dates back some 3 centuries. As early as the mid-17th century, van Helmont observed that a willow tree grew from 5 lb to over 570 lb in 5 years while the soil it was planted in decreased in weight by only about 1 lb He postulated that most of the tree's mass must have come from the water that had been added to the soil [1]. In 1771 Joseph Priestly, who discovered the existence of oxygen, demonstrated that a mouse could not survive in an enclosed glass container that had previously been burned out by a flame. But if a sprig of mint was placed in the container for a few days, the mouse could survive [2]. In the late 18th century Ingenhousz and Senebier demonstrated that it was the green portion of plants that had the ability to "fix air" and the process required carbon dioxide. By the mid 19th century it was known that this energy of sunlight was responsible for the formation of sugars in plants. It was C. B. van Niel in the 1920's , studying photosynthetic bacteria, that first proposed that photosynthesis consisted of a pair of oxidizing and reducing processes. The light reaction was mediated by chlorophyll or bacteriochlorophyll and generated the primary oxidizing and reducing entities. These would then oxidize the primary electron donor (H_2O in plants, H_2S or reduced organic compounds in bacteria) and reduce the electron acceptor (CO_2 in plants). This view of the photochemistry being a separation of oxidizing and reducing elements in the presence of light and mediated by chlorophyll pigments is central to our present day view of photosynthesis [1].

Overview

Photosynthesis is the process by which light is converted into chemical energy for biosynthetic purposes. Photosynthetic organisms are the primary producers for all major ecosystems on this planet, and as such, represent the ultimate source of energy and food for nearly all life. Furthermore, most of our industrial energy requirements are provided by photosynthetically generated biomass in the form of fossil fuels. Photosynthesis has quite literally changed the atmosphere of the earth from one of reducing power to one of oxidizing power.

Both eucaryotic and procaryotic photosynthetic organisms are known to occur. The photosynthetic eucaryotes include green plants, algae, and phytoplankton. The photosynthetic procaryotes include blue-green algae, green sulfur bacteria, and purple nonsulfur bacteria. The procaryotes represent a more primitive group of organisms and it is thought that photosynthetic bacteria arose earlier than eucaryotic photosynthetic organisms. Indeed, present serial endosymbiotic theories maintain that photosynthetic procaryotes were probably the progenitors of the eucaryotic cellular organelle, the chloroplast, which is responsible for higher plant photosynthesis.

The overall process of photosynthesis in plants can be represented by

$$6CO_2 + 6H_2O \xrightarrow{\text{light}} (CH_2O)_6 + 6O_2 \tag{1.1}$$

This equation represents a complicated series of transformations that can be divided into two major phases; the light and dark phases. The light phase represents the series of reactions that are dependant on the presence of light and are thus photochemical in nature. In this phase, the photosynthetic organism utilizes the energy of light from the visible and near infrared region of the spectrum to drive a series of electron transfer steps that culminates in a separation of charge across the photosynthetic membrane. Chlorophyll (Chl) and bacteriochlorophyll (BChl) pigments are central to these light harvesting and electron transport processes, and are ubiquitous to all known photosynthetic organisms.

This charge separation process occurs in the photosystem (PS) complex. A photosystem can be defined as a membrane bound, chlorophyll containing, pigment-protein complex that is capable of carrying out light induced charge separation across the membrane. Plants contain two PS complexes, PSI and PSII, while bacteria contain only one PS. Associated with the PS are other membrane specific chlorophyll containing proteins known as antenna proteins (AP). The AP typically absorb energy at a higher wavelength than the PS and are not capable of light induced charge separation. When the pigments in the AP are excited by light, the energy is rapidly transferred via nonradiative processes to the PS where the charge separation steps are initiated. In plants there are roughly 250 loosely associated Chl molecules (presumably in AP) for every PSI/PSII pair [3]. In the purple photosynthetic bacterium *Rhodopseudomonas sphaeroides* there are two major AP, B875 and B800–850, named for their long wavelength absorption maxima. B875 occurs in a nearly constant ratio of 15:1 with the PS, while B800–850's membrane concentration varies inversely with the incident light intensity [4]. Other accessory pigments, such as carotenoids, are present as well and together with the antenna proteins act to extend the sensitivity of the photosynthetic process in the visible region of the spectrum. The sequence of the primary charge separation steps in a PS can be represented as

$$\begin{aligned} DA_1A_2A_3 \overset{\text{light}}{\rightarrow} D^*A_1A_2A_3 &\rightarrow D^+A_1^-A_2A_3 \\ &\rightarrow D^+A_1A_2^-A_3 \rightarrow D^+A_1A_2A_3^- \end{aligned} \tag{1.2}$$

Here D is the light absorbing center and primary electron donor (excited either directly or by energy transfer from the AP) in the PS, while A_1, A_2, and A_3 are the electron acceptors. In the bacterial PS, D is known to be a dimer of BChl molecules and the acceptors are known to be comprised of both bacteriopheophytin (a BChl with the central Mg replaced by two protons on opposite pyrrole nitrogens) and quinone moieties. In plants the PSI/PSII pair act in concert to form the electron transport chain represented in Figure 1.1.

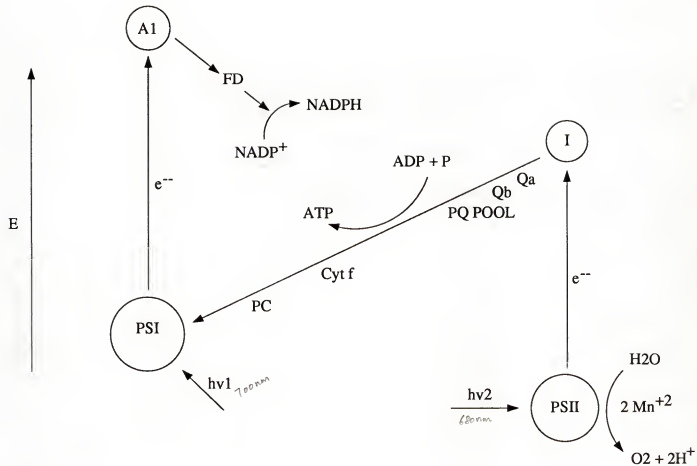

Figure 1.1 Path for electron flow for PSI and PSII in eucaryotic photosynthesis. Flow starts from water and ends in NADPH. Abbreviations are Qa, Qb = quinone acceptors a and b respectively, PQ POOL = plastoquinone pool, Cytf = cytochrome f, PC = plastocyanin, FD = ferredoxin, $NADP^+(H)$ = nicotinamide adenine dinucleotide phosphate (reduced) ADP (ATP) = adenosine di- (tri-) phosphate. Visible light hv1 and hv2 are known to have wavelengths of roughly 700 nm and 680 nm respectively. Reproduced from[1, 5].

The absorbing center in PSI contains chlorophyll-a (Chla) which may be a dimer similar to the bacterial PS. PSI absorbs light at about 700 nm and transfers an electron to an acceptor, A_1, of uncertain identity, possibly an FeS protein. Due to the characteristic light-absorption changes at 430 nm upon reduction, acceptor A_1 has also been referred

to as P430. From there the electron ends up (possibly through other oxidized/reduced electron carriers) on an FeS center in the protein ferredoxin (FD) where, in the presence of the flavoprotein enzyme ferredoxin-NADP oxidoreductase, it reduces oxidized nicotinamide adenine dinucleotide phosphate ($NADP^+$) to NADPH. In PSII the primary donor, containing Chla, is excited at about 680 nm and transfers an electron to the primary acceptor I. The identity of the acceptor I is not confirmed but is thought to be a pheophytin based upon spectral changes observed at 550 nm From there the electron is transported via two quinones, Qa and Qb (a two electron process), to the plastoquinone pool (PQ Pool) cytochrome f (Cyt f) and plastocyanin (PC, a blue Cu containing protein) where it ultimately reduces the Chla in PSI. This series of electron transport reactions is capable of carrying out the photophosphorylation of adenosine di-phosphate (ADP) to its tri-phosphate form (ATP). It is the formation of the high energy phosphate bond in ATP that essentially stores much of the biochemically available energy from the light driven steps. PSII is reduced by transport of electrons from the oxidation of H_2O. This transformation is poorly understood but is known to require Mn^{2+} [5]. The spatial relationships of the electron carriers in the above scheme are certainly more complicated than presented here. The structural details of these proteins and protein-pigment complexes are not well known. Rather their functional relationships have been discerned from decades of elegant biochemical and biophysical studies [1]. Only recently has PSI from spinach chloroplasts been successfully crystallized [6].

The dark phase, which does not require the presence of light, is the series of reactions that utilize the cofactors formed from the electron transport such as adenosine tri-phosphate (ATP) and reduced nicotinamide adenine dinucleotide phosphate (NADPH). These cofactors are required in many of the biosynthetic reactions of the photosynthetic organism, such as the reduction and incorporation of carbon dioxide into carbohydrates. The process of fixing carbon dioxide into biochemical carbon is a complicated series of transformations that varies with plant species. The C_3 plants, occurring mainly in

temperate regions, first fix CO_2 into 3–phosophoglycerate, then ultimately, via the Calvin cycle, to hexose. The C_4 plants, mainly tropical, fix CO_2 into the 4 carbon organic acid oxaloacetate and ultimately into hexose via the Hatch-Slack pathway [5]. It is the light phase reactions, specifically those of photosynthetic bacteria, that are further addressed in this dissertation.

Bacterial Photosynthesis

Bacterial photosynthesis is simpler than eucaryotic photosynthesis. Indeed most of our detailed information on photosynthesis comes from a few well described bacterial systems. The bacterial RC is a multiple subunit, globular membrane protein-pigment complex. In December 1984 Deisenhofer, Epp, Miki, Huber, and Michel published the 3.0 Å resolution X-ray crystal structure of the PS from the purple nonsulfur bacterium *Rhodopseudomonas viridis* [7, 8], an achievement for which J. Deisenhofer, R. Huber, and H. Michel were later awarded the 1988 Nobel Prize in Chemistry. The structure has further been refined to 2.3 Å resolution [9]. Later the X-ray crystal structure for the PS from *Rb. sphaeroides* was also solved [10]. These PS are commonly referred to as photosynthetic reaction centers (RC). Both RC were shown to contain four BChls, two bacteriopheophytins (BPhs) two quinones, and a nonheme Fe(II). Specifically in *Rps. viridis* these are bacteriochlorolphyll-b (BChlb) and bacteriopheophytin-b (BPhb) while *Rb. sphaeroides* contains bacteriochlorophyll-a (BChla) and bacteriopheophytin-a (BPha) Figure 1.2. While there are some differences in the details of these two RC, the overall structure, optical properties, and electron transfer dynamics are quite analogous. The X-ray structure of the RC from *Rps. viridis* is more highly refined and studies done in this dissertation were performed on these X-ray coordinates. Where applicable, reference will be made to distinctions between the *Rps viridis* and *Rb. sphaeroides* RC. The structural arrangement of the chromophores the *Rps. viridis* RC is shown in Figure 1.3.

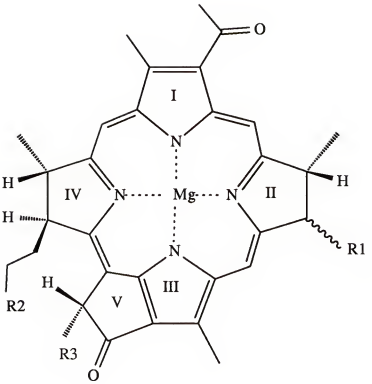

Figure 1.2 Bacteriochlorophyll-b (BChlb) and bacteriochlorophyll-a (BChla). Abbreviations: R1 ethyl (BChla) or ethylidine (BChlb) R2 phytol side chain, R3 CO_2CH_3. The corresponding pheophytin derivatives have the central Mg replaced by two protons attached to the ring I and III nitrogens.

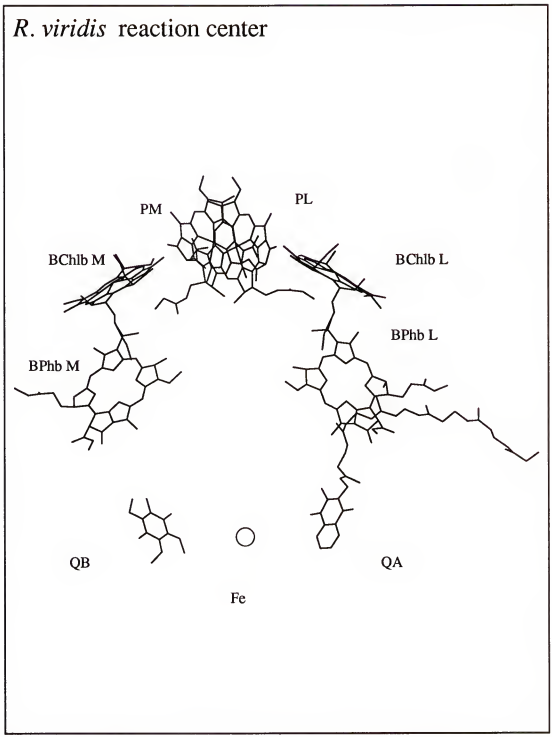

Figure 1.3 The chromophores of the photosynthetic[9]. Abbreviations are: P_M, P_L = M and L BChlb moieties of the special pair dimer, $BChlb_M$, $BChlb_L$ = M and L auxiliary BChlb, $BPhb_M$, $BPhb_L$ = M and L BPhb, Q_A = quinone A is a menaquinone, Q_B = quinone B is a ubiquinone, Fe = the nonheme iron atom. The periplasmic (extracellular) side at the top of the figure and the cytoplasmic (intracellular) side at the bottom.

The surrounding protein (not shown) is composed of three subunits; labelled as L, M, and H for light, medium, and heavy. These three subunits together contain 11 membrane spanning α–helices that form a barrel-like structure around the chromophores providing a scaffold for holding them in place. The chromophores form two branches with the BChlb and BPhb of both branches labelled as to their major association with either the L or M subunits. At the top of the structure there is a dimer of BChlb molecules that are closely juxtaposed with their pyrrole rings I overlapping at an average macrocycle separation of about 3.3 Å. This structure is known as the special pair (P) and is the primary electron donor in the light induced charge separation process. Adjacent to P the remaining chromophores form two branches exhibiting an approximate C2 symmetry about an axis extending from the Fe(II) atom to P. Each branch consists of a proximal auxiliary BChlb ($BChlb_M$, $BChlb_L$) and a distal BPhb ($BPhb_M$, $BPhb_L$). Surprisingly, only the L-branch is known to be photosynthetically active with relative rates of L-branch: M-branch electron transfer being estimated from 20–200 [11]. The nonheme Fe(II) atom is ligated by four histidine residues one from each of four α-helices, and the bidentate carboxyl group from a nearby glutamic acid residue. In *Rps. viridis* there is a bound cytochrome lipo-protein containing four Fe-hemes that is attached to the periplasmic side of the RC (not shown). The cytochrome acts as the secondary electron donor *vide infra*. In *R. sphaeroides* a soluble cytochrome-c protein that resides in the periplasmic space fulfills this role.

Based on a large body of experimental and theoretical work (for reviews [12–14]) the overall process of electron transport can be described. In *Rps. viridis* the BChlb dimer (P) has a long wavelength absorption maximum at 960 nm at physiological temperatures. When P is excited, either directly or by energy transfer from the AP, it rapidly transfers an electron to $BPhb_L$ (Figure 1.3) in about 1 ps. The electron is then transferred to the quinone, Q_A (the secondary acceptor) in about 200 ps. The rate constant for this reaction is also weakly temperature dependant. The electron subsequently is transferred to the

ubiquinone Q_B which picks up a proton forming a semi-quinone. This reduction occurs in about 100 μs. The photo-oxidized P is reduced by the membrane bound cytochrome protein on a millisecond timescale, *vide supra*. The reduction of Q_B occurs twice to form the double reduced ubiquinol. This ubiquinol then diffuses into the cytoplasmic quinone pool and is replaced by an oxidized ubiquinone. The role of the Fe(II) atom is not clear, though it has been known for some time that it is not involved as an electron carrier[15]. There are conflicting reports of the role of the Fe(II) atom in stabilizing the structural integrity of the Q_A, Q_B sites, and as having an electrostatic effect on Q_A –> Q_B electron transfer[15, 16]. Based on ESR data, the existence of P as the primary electron donor was proposed long before the X-ray structure was solved [17, 18]. Similarly, the identity of a BPh as the primary acceptor was also proposed based on ESR data[19]. Thus it was surprising to see not only two branches in the RC (only one of which is active) but the existence of an auxiliary BChl between the primary donor (P) and the primary acceptor (BPh_L). The vectorial nature of electron transport along only the L-branch, as well as the role of the auxiliary BChl in the primary electron transfer step, is presently not understood, and both remain the object of intensive investigation.

Primary Electron Transfer

The primary electron transfer event (PET) $P^*BPh_LQ_A \rightarrow P^+BPh_L^-Q_A$, is very fast, exhibits a quantum yield of about 1.0 over a broad range of temperatures, and is essentially irreversible[20–23]. The secondary electron transfer event, $P^+BPh_L^-Q_A \rightarrow P^+BPh_LQ_A^-$, is also known to be nearly temperature independent. The structural and dynamic properties of the RC that control such a reaction are not well understood. Furthermore, why is only one branch of the RC photosynthetically active, and what role, if any, does the auxiliary BChl fulfill?

The rate of ET between a donor and acceptor depends upon the overlap of electronic densities and a nuclear vibration overlap factor[24]. An expression for a nonadiabatic multiphonon ET rate constant can be derived[20, 24] and is given as

$$k = \frac{2\pi}{\hbar} H_{AB}^2 \, (FC) \tag{1.3}$$

Here H_{AB} is the electronic matrix element coupling between the donor-acceptor precursor state, DA, and the donor-acceptor successor state D^+A^-, and FC is the nuclear piece or thermally averaged Franck-Condon factor which represents the sum of products of overlap integrals of the vibration and solvation of the reactants and the medium[24]. The electronic factor is thought to fall off as $e^{-\beta r}$ with β typically being about 1.2 $Å^{-1}$ for a typical protein environment[24, 13]. and is highly dependant upon the relative orientation of the donor-acceptor pair. The FC factor depends upon the free energy change of the reaction as well as the reorganization energy, both of which depend not only on the nature of the donor-acceptor precursor and successor complexes but also upon the environment or solvent. The solvent in the case of the RC is the protein surrounding the chromophores, as well as possibly a few water molecules. Theory tells us that a reaction in which the reorganization energy equals the free energy change for the forward reaction should exhibit little or no temperature dependance[24]. This is because the FC factor is optimal, or the system needs little or no change in the nuclear positions to prepare it for the ET

event. Thus it is thought that the both the PET and the secondary ET are activationless (or nearly so) based upon their relative insensitivity of their rates to temperature. The rate constant for *Rps. viridis* PET event varies from $(2.8\ \text{ps.})^{-1}$ to $(0.7\ \text{ps.})^{-1}$ over the temperature range 300–8 K[21]. In *Rb. sphaeroides* P^* is about 1.4 eV above the ground state. From fluorescence experiments the state P^+Bph^- is estimated to be about 0.15–0.20 eV in free energy below P^*[25, 26]. Thus, assuming a nearly activationless PET event (FC $\approx$ 1.0, eqn. 1.3) we expect the reorganization energy to be about 0.15–0.20 eV as well. Estimates of the internal reorganization energy for tetrapyrrole pigments of about 0.1 eV have been made[24, 27]. Assuming the simplest case where the closest edge to edge distance of the macrocycles of P and BPh is about 8 Å, and β = 1.2 Å^{-1}, then equation 1.3 gives us an estimated rate constant for the PET of about $(1\ \text{ns.})^{-1}$, which is much slower than the experimentally observed rate constant of $(0.7 - 2.8\ \text{ps.})^{-1}$[13]. This observation has been used to imply a mediating role for the $BChl_L$ in the PET event.

There have been several mechanistic descriptions proposed for the PET, all of which assign some role to the auxiliary $BChl_L$[26, 28–31, 20, 32, 33]. The two most widely considered mechanisms are

1. $BChl_L$ is an explicit intermediate (EI).

$$P^*\ BChl_L\ BPh_L \overset{k_1}{\rightarrow} P^+\ BChl_L^-\ BPh_L \overset{k_2}{\rightarrow} P^+\ BChl_L\ BPh_L^- \qquad (1.4)$$

   [28, 34]

2. $BChl_L$ mediating ET from P to BPh_L via superexchange coupling (SEC)[29–31, 20, 32]. In this mechanism $P^+\ BChl_L^-$ is higher in energy than P^* and acts to enhance the electronic coupling between $P^*\ -\ BPh_L$.

The presence of $BChl_L^-$ has not been detected experimentally in femtosecond measurements.[22, 21] The EI mechanism, however, could involve $BChl_L^-$ as an intermediate where $k_2 >> k_1$ (eqn. 1.4). If the EI model is valid, then recent measurements by Fleming, Martin, and Breton estimate $k_2 \approx$ 50–100 times k_1 which would make $k_2 \approx$

10 fs[21]. Rates this fast are outside the realm of conventional ET theory. The nonadiabatic/adiabatic model is a modification of the EI model in which the first step is nonadiabatic and rate determining and the second ultrafast step is adiabatic[34]. The SEC mechanism is able to explain the lack of observable bleaching of $BChl_L$. However, theoretical calculations require relatively large off-diagonal coupling matrix elements between the states P^*, $P^+ BChl_L^-$, and $P^+ BPh_L^-$[30]. These large off-diagonal coupling elements have been shown by Marcus to be inconsistent with the experimentally observed singlet-triplet splitting of the radical pair, $P^+ BPh_L^-$[34]. Both of these mechanisms remain unproven. The RC is a large and complex system, and the debate on these ET mechanisms will probably continue for some time.

CHAPTER 2
ELECTROCHROMIC EFFECTS

Introduction

The electrochromic effects of point charges on the long wavelength absorption maxima of bacteriochlorophyll-a, -b, and -g (BChla, BChlb, BChlg respectively) and (pyrro)chlorophyll-a ((p)Chla) have been systematically examined using the INDO/S method. A distinctive pattern of shifts common to all these molecules emerges. Both red and blue optical shifts are predicted. The sign and magnitude of these shifts depend upon the sign of the point charge (positive or negative) and its location. A positive charge in the vicinity of ring I induces a large red shift; a negative charge, a large blue shift. A positive charge in the vicinity of rings III and V, however, produces a large blue shift and a negative charge, a large red shift. In general, the ordering of the magnitudes of the electrochromic response is BChlg > BChlb > BChla > (p)Chla for analogous placement of charges. All our results are explained by a qualitative model that considers the distribution of electron density in the ground and excited states and the dipole moment differences between these states.

The primary electron transfer and migration events of photosynthesis create cations and anions in close proximity to BChls and bacteriopheophytins (BPhs)[7, 8, 10, 21, 23, 22]. Calculations of the electrochromic effects of these charged species on the accessory BChls and BPhs in bacterial reaction centers of known structure yield trends consistent with some of the spectral changes observed after photoexcitation or during steady-state trapping experiments[35–37].

Methods

Spectroscopic INDO (INDO/S)[38–40] is a semi-empirical method, based on the intermediate neglect of differential overlap (INDO) approximation of Pople and coworkers[41–44]. An electronic spectrum is calculated from the self-consistent field (SCF) ground state by performing a configuration interaction (CI) of a specified number of single excited determinants. For the calculations reported here, the CI included the lowest 121 singly excited configurations. Point charges are not represented by basis functions, rather, they are included into the Hamiltonian through the diagonal one-electron terms.

$$V_{\overline{\mu}\,\overline{\mu}} = \sum_{\mu} P_{\mu\mu} \langle \overline{\mu} | \frac{Z_p}{R_{1p}} | \overline{\mu} \rangle \tag{2.1}$$

Here $\overline{\mu}$ indicates functions of full spherical (s-type) symmetry that are required to maintain the rotational invariance of the INDO Hamiltonian, *P* represents the charge and bond order matrix in the zero differential overlap (ZDO) basis, Z_p is the charge of the point charge, and R_{1p} is the distance of the electron from the point charge. Consistent with the INDO model, no terms of the type $\langle \mu | \frac{Z_p}{R_{1p}} | \nu \rangle$ are included in the off-diagonal elements of the one-electron matrix.

The geometries of the BChls, -a, -b, and -g, BPhb, and pyrro-chlorophyll-a (pChla) were based on the crystal structure coordinates of ethylchlorophyllide-a[45]. Appropriate adjustments were made for the different ring substituents of the various species. Figure 2.4 shows the models used in the calculations and gives the numbering. Results are presented for BChls -a and -b with the 3–acetyl group 90° out of the mean plane of the four pyrrole nitrogens. pChla has two protons rather than a proton and a carbomethoxy group off ring V. BPh has protons bound to N1 and N3 rather than a central Mg.

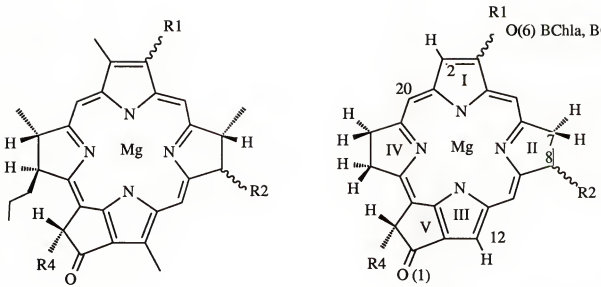

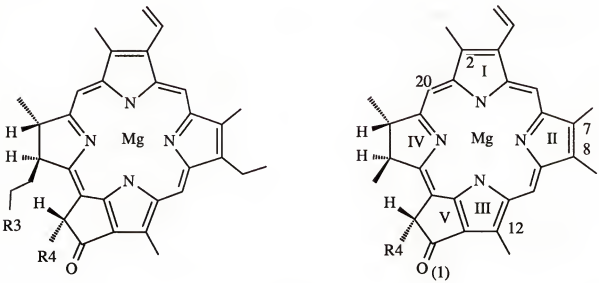

Figure 2.4 Molecules used in this study. The top pair represent bacteriochlorophylls –a, –b, and –g, and the bottom pair (p)chlorophyll-a. For each pair the structure on the left is the actual molecule while the structure on the right is the structure used in this study. Abbreviations are: R1 acetyl (BChla and BChlb) $-CH=CH_2$ (BChlg); R2 ethyl (BChla) ethylidine (BChlb and BChlg); R3 phytol; R4 CO_2CH_3. The atomic numbering for the model structures is that used in the text and tables. The numbering of the nitrogens corresponds to their respective rings (i.e. N1 is on ring I).

Results and Discussion

Table 2.1 presents the electrochromic effects calculated for BChls -a, -b, and -g and (p)Chl when a single positive or negative point charge is systematically placed 3.5 Å above various atoms. The charge-induced frequency, $\Delta\nu$, and oscillator strength, Δf, shifts of the lowest singlet transition (the Q_y transition) are given. A negative transition $\Delta\nu$ indicates that the charge has lowered the energy of the Q_y transition so that it absorbs at a longer or red shifted wavelength. A positive $\Delta\nu$ indicates a blue shift relative to no charge. Likewise, a positive Δf denotes an increase in the oscillator strength whereas a negative sign denotes a decrease. Note that the Δf values are inversely coupled to those of $\Delta\nu$, except in cases where $\Delta\nu$ is very small. That is to say, for the Q_y transition, the oscillator strengths increase for red shifts and decrease for blue shifts. These corresponding trends in transition energy and oscillator strength can be understood in terms of Gouterman's four-orbital model[46]. In D4h porphyrin the near degeneracy of the two y-polarized single electron promotions (HOMO-LUMO and HOMO-1 – LUMO+1, both have similar oscillator strengths) causes them to mix strongly in the CI. The result of this is that the two states split with the higher energy (soret or By) band containing nearly all the oscillator strength while the lower Qy band has little or no oscillator strength. In chlorins, bacteriochlorins, and their derivatives, the HOMO-LUMO gap is reduced relative to D4h porphyrin, and thus the near degeneracy of the two y-polarized single electron promotions is lifted. The interaction of these two y-polarized configurations is reduced relative to D4h porphyrin, and thus the partial cancellation of oscillator strength in the Qy band is also reduced. The net effect of this is that the Qy band now appears to 'borrow' intensity from the By band. In (B)Chls the Q_y transition is dominated by the HOMO-LUMO gap. A perturbation that modifies the HOMO-LUMO gap will have direct effects on the absorption maximum and intensity of the Q_y band through the interaction of the two y-polarized configurations. Thus we observe a red shift (caused by the point charges used in this study) results in a decrease in the HOMO-

LUMO gap and consequently the partial cancellation of oscillator strength in the CI is reduced relative to the unperturbed system. This gives the red shifted Q_y transition a larger oscillator strength. The reverse applies to the blue shifted Q_y transitions, as the increased cancellation of oscillator strength between the above two configurations is enhanced when the HOMO-LUMO gap is increased. A more systematic and physical description of these effects is delineated below.

Table 2.1 Effect of Point Charges on the Q_y Band of (B)Chls.

Point Charge (a.u.)	Position[a]	Δf[b]	$\Delta\nu$ (cm^{-1})[c]				
		BChlg	BChlg	BChlb	BChla	pChla	Chla
+1	N1	0.099	-1510	-1440	-1053	-716	
-1		-0.050	2291	2297	2014	591	
+1	N2	-0.022	-205	-239	-51	34	
-1		0.026	21	109	-5	-84	
+1	N3	-0.096	1502	1329	1579	623	
-1		0.126	-1109	-895	-962	-635	
+1	N4	-0.021	-551	-564	-224	41	
-1		0.031	439	440	182	-159	
+1	C20	0.092	-1341	-1272	-866	-634	
-1		-0.059	2066	1993	1669	303	
+1	C2	0.170	-1754	-1603	-1229	-1187	-1145
-1		-0.085	2919	2872	2617	782	770
+1	O6		NA[d]	-1256	-1103	NA	
-1				1886	1726		
+1	C7	-0.002	49			135	
-1		-0.018	-243			-38	
+1	C8	-0.041	796	712	519	-26	
-1		0.031	-1204	-1059	-645	-294	
+1	C12	-0.080	2772	2579	2709	995	
-1		0.139	-1472	-1160	-1079	-728	
+1	O1	-0.074	1937	1796	1958	1002	1024
-1		0.098	-1110	-1000	-895	-583	-626

a: The charge is 3.5 Å above the atom. The numbering is given in Figure 2.4.

b: Shift in oscillator strength relative to no charge. A positive value indicates an increase; a negative value, a decrease in Q_y intensity. The reference value for the Q_y transition of BChlg is 0.517.

c: Shift in frequency relative to no charge. A positive value denotes a blue shift; a negative value, a red shift in the Q_y transition energy. The reference energies for BChlg, BChlb, BChla, pChla, and Chla are 13773 cm^{-1}, 13663 cm^{-1}, 13610 cm^{-1}, 15419 cm^{-1}, and 15532 cm^{-1}, respectively.

d: Not applicable due to structural differences.

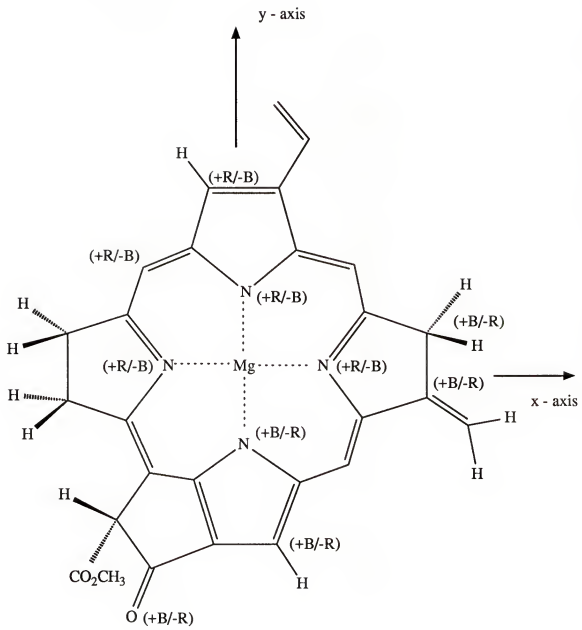

Figure 2.5 Pattern of electrochromic shifts for the Q_y band for bacteriochlorophyll-g. Point charges were +/- 1.0 au charges placed 3.5 Å above the indicated atoms. Abbreviations: (+B/-R) +1.0 charge gave blue shift, -1.0 charge gave red shift; (+R/-B) +1.0 charge gave red shift, -1.0 charge gave blue shift. The numerical results for these atomic positions are given in Table 2.1. See Figure 2.4 for numbering of atomic positions and rings.

Points of opposite charge placed at the same location induce shifts of opposite

magnitude. A distinctive pattern for the Q_y shifts, common to all the molecules, emerges and is illustrated in Figure 2.5 for BChlg. This pattern depends on the sign of the charge and its location. Figure 2.5 shows that a positive charge in the vicinity of ring I induces a red shift whereas a positive charge near rings III or V gives a blue shift. The shift pattern is exactly the opposite for a negative charge (Figure 2.5). Thus, the effect of a charge of the same sign reverses about a line passing roughly along the molecular x-axis. As seen from Table 2.1, the magnitude of $\Delta\nu$ is related to the position of the point charge relative to the y-axis. A charge near the x-axis gives a much smaller $\Delta\nu$ than a charge on or near the y-axis. At many positions, the electrochromic response is BChlg > BChlb > BChla > (p)Chla.

Electrochromic shifts have been observed experimentally in systems where protonated Schiff base groups were attached to the macrocycles of porphyrins and chlorins at various positions[47]. INDO/S-CI calculations on these species agree with experiment, Table 2.2[47]. Davis et al. [48] changed the C7 substituent of pChl to an amino group. Protonation of this group resulted in a blue shift of 90 cm^{-1}, to be compared with the 135 cm^{-1} blue shift predicted by placing a +1 point charge above C7 of pChla (Table 2.1). The size of the shift is small. However, note that the charged group is located near the predicted crossover region (Figures 2.4 and 2.5).

Table 2.2 Effect of a Covalently Bound Charged Group (Protonated Schiff Base) on the Q_y Band of (B)Chls.

Schiff Base	$\Delta\nu$ (cm^{-1})[b]			
Position[a]	BChlg	BChlb	BChla	pChla
O6 (25 deg. to ring I)	NA[c]	-2319	-1971	NA
O6 (90 deg. to ring I)			-2090	
O1	2614	2399	2604	1490

a: The carbonyl that has been replaced by either =NR or =NRH$^+$ groups (R = CH_3).
b: Frequency shift of the protonated Schiff base (=NRH$^+$) relative to the unprotonated Schiff base (=NR).
c: Not applicable due to structural differences.

All the predicted electrochromic effects can be explained in terms of a qualitative model developed in the next section. These effects are shown to result from the strong y-polarization of the Q_y transition (the y-axis passes through rings I and III) and the large difference between the calculated ground and Q_y dipole moments.

Theory

The electrochromic shift behavior of the (B)Chl Q_y band can be understood in terms of the distribution of electron density within the ground and first excited states in terms of their respective dipole moments. Table 2.3 gives the calculated dipole moments for the ground state (μ_o) and the Q_y state (μ_{Qy}) for the (B)Chls in the absence of point charges along with the difference in dipole moment between the two states ($\Delta\mu$). The dipole moment vector points in the direction of net positive charge. In the ground state the electron density is higher in the ring III region than the ring I region. The calculated Q_y transition results in a net shift in electron density along the y-axis from ring III to ring I. This is reflected in the large positive μ_y value for the ground state and the small μ_y value for Q_y.

Table 2.3 Calculated State Dipoles [a]

Molecule	State	μ_x [b]	μ_y	μ_z
	ground state	-0.1256	13.6710	0.3203
BChlg	Q_y	1.7287	1.2652	0.3391
	$\Delta\mu$ [c]	1.8543	-12.4058	0.0188
	ground state	-1.3464	10.8295	4.0070
BChlb	Q_y	0.5019	-0.8447	3.9985
	$\Delta\mu$	1.8483	-11.6742	-0.0085
	ground state	-0.0860	10.3297	3.9951
BChla	Q_y	0.2572	-0.7976	3.9351
	$\Delta\mu$	0.3432	-11.1273	-0.0600
	ground state	0.6811	6.4990	-0.4502
pChla	Q_y	-1.5782	1.5312	-0.3418
	$\Delta\mu$	-2.2593	-4.9678	0.1084
	ground state	0.5525	8.7094	0.6642
Chla	Q_y	0.4211	5.3424	0.5991
	$\Delta\mu$	-0.1314	-3.3666	-0.0651

a: Values listed are obtained from INDO/S-CI calculations of the unperturbed molecules.
b: Debyes
c: Excited state (Q_y) minus the ground state dipole moments.

Figure 2.6 schematically shows the changes in the calculated energies of the ground and Q_y states when a point charge is placed 3.5 Å above rings I and III. Also shown are the relative magnitudes of the y-component of μ_o and μ_{Qy} for unperturbed (no charge present) BChlg. A positive charge lowers the energy of both states. When placed near the "head" of the dipole moment vectors (ring I) the charge depresses the energy of the Q_y state more than the ground state. The Q_y state has more electron density near the ring I region relative to the ground state and therefore its stabilizing interaction with a positive charge is larger. $E_I^+ < E_o$ (Figure 2.6) results in a red shift. Conversely, a positive charge near the "tail" of the dipole moment vectors (ring III) depresses the energy of the ground state more than the Q_y state because the ground state has relatively

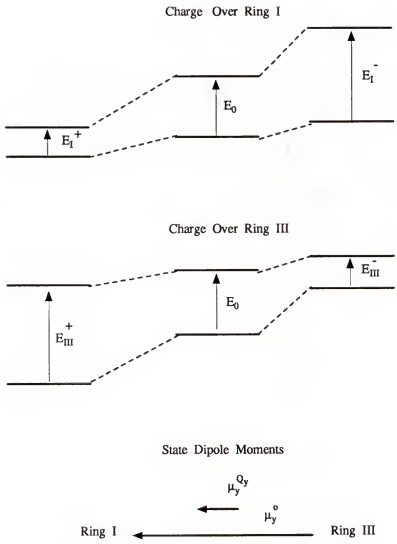

Figure 2.6 Schematic representation of the effect of point charges placed over rings I and III on the Q_y transition of (B)(p)Chls. Abbreviations are E_0; the Q_y transition energy in absence of point charges, $E^{+(-)}{}_I$ the Q_y transition energy in the presence of a positive (negative) point charge over ring I, and $E^{+(-)}{}_{III}$ the Q_y transition energy in the presence of a positive (negative) point charge over ring III. Schematic representation of the state dipole moments for the y-components of the ground state (μ_o) and Q_y state (μ_{Qy}) in the absence of any point charge perturbations is given at bottom of figure. In both cases the dipole moments point from the ring III to the ring I side of the macrocycle. The Q_y state exhibits a net shift of electron charge density towards ring I and hence its state dipole moment is smaller than the ground state.

greater electron density near the ring III region. $E^{+}_{III} > E_o$ (Figure 2.6) results in a blue shift. Negative charges induce shifts opposite to those of positive charges because of their energetically destabilizing interactions with regions of high electron density. A negative charge raises the energies of both states, the state with relatively more electron density in the vicinity of the negative charge is raised the most. Thus, a negative charge near the ring I region raises the energy of the Q_y state more than the ground state ($E^{-}_{I} > E_o$, Figure 2.6) resulting in a blue shift. A negative charge near ring III, however, raises the energy of the ground state more than the Q_y state ($E^{-}_{III} < E_o$, Figure 2.6) and the calculated transition is red shifted.

At the point charge-atomic center distances used in this study, a positive charge always differentially lowers the energies of both states while the negative charge raises these energies. Yet it is the orientation of the point charge relative to μ_o and μ_{Qy} that determines whether the electrochromic shift is a red or blue shift. This demonstrates why a given charge gives Q_y electrochromic shifts of opposite sign on different sides of the molecular x-axis and suggests a point charge-dipole interaction as a first order indicator of the electrochromic response of the system to the point charge.

The point charge is represented as a fixed point with no associated basis functions. As such it creates an inhomogeneous electric field that perturbs the molecular electronic distribution during the SCF process. Fock matrix elements, F', are given for a closed shell (RHF) system by

$$F'_{\mu\nu} = H'_{\mu\nu} + \sum_{\lambda,\sigma} P'_{\lambda\sigma}[(\mu\nu|\lambda\sigma) - \frac{1}{2}(\mu\lambda|\sigma\nu)] \tag{2.2}$$

where H', and P' are the one electron Hamiltonian and charge and bond order matrix, respectively, in the presence of the point charge.

$$H'_{\mu\nu} = H_{\mu\nu} + P_{\mu\nu}(\nu|\frac{Z_p}{R_{1p}}|\mu) \; = \; H_{\mu\nu} + V'_{\mu\nu} \tag{2.3}$$

The second term of eqn. 2.3 represents the perturbation by a point of charge Z_p. The total energy of a single determinant SCF wavefunction obtained by solution of the above

equations is given by.

$$E = \frac{1}{2} Tr P'(F' + H') + \sum_{A<B}^{nuclei} \frac{Z_A Z_B}{R_{AB}} + \sum_{A}^{nuclei} \frac{Z_A Z_p}{R_{Ap}} \tag{2.4}$$

The primed matrices include all the effects of the point charge (electronic relaxations relative to the unperturbed calculation). The nuclear-nuclear and nuclear-point charge repulsion terms are fixed additive constants. Since a single one-electron promotion dominates the description of the (B)Chl Q_y state, eqn. 2.4 is appropriate for estimating the energies of the Q_y transition.

If, in addition, we assume that the perturbation from the point charge is small and examine only the first order terms, then from eqn. 2.4 we can obtain an expression for the Q_y transition energy in the presence of a single point charge.

$$\Delta E + \delta E^1 = (E^o_{Qy} - E^o_o) + \delta V_{pe} \tag{2.5}$$

where ΔE is the spectroscopic transition energy in the absence of the perturbing point charge and δE^1 is the first order electrochromic shift due to the point charge (eqn. 2.6).

$$\delta E^1 = \delta V_{pe} = \sum_{\mu\nu} \delta P_{\mu\nu} (\nu | \frac{Z_p}{R_{1p}} | \mu) \tag{2.6}$$

Here δP is the difference in the charge and bond order matrix between the ground state and the dominant determinant from the Q_y state. All nuclear-nuclear and point charge-nuclear terms cancel. Under the assumptions of the INDO method

$$(\nu | \frac{Z_p}{R_{1p}} | \mu) = \delta_{\mu\nu} (\mu | \frac{Z_p}{R_{1p}} | \mu) \tag{2.7}$$

Thus we can rewrite the expression for the electrochromic shift, eqn. 2.6, as

$$\delta E^1 = Z_p \sum_{\mu} \delta P_{\mu\mu} (\overline{\mu} | \frac{1}{R_{1p}} | \overline{\mu}) \tag{2.8}$$

where $\overline{\mu}$ designates basis functions of full spherical symmetry. The validity of eqn. 2.8 as an approximation to the electrochromic response depends upon the magnitude of the charge, its distance from the molecule, and the higher order response of the molecule

(through P) to the electric field of the point charge (ie., its polarizability). Equation 2.8 essentially describes the interaction of a point charge with the difference in the electronic contribution to the dipole moment between the ground state and the Q_y state.

Table 2.4 shows the calculated values of μ_o and μ_{Qy} for BChlg in the presence of point charges over N(I) and N(III). The contribution of the point charge, itself, has been subtracted.

Table 2.4 Effects of Point Charges on the State Dipole Moments of BChlg.

Point Charge (a.u.)	Position[a]	State	μ_x	μ_y	μ_z
		ground state	0.0180	6.7151	0.0375
+1	N1	Q_y	1.9228	-0.3027	0.0459
		$\Delta\mu$[c]	1.9048	-7.0178	0.0084
		ground state	-0.1535	18.9081	0.6331
-1	N1	Q_y	1.4240	4.6776	0.6613
		$\Delta\mu$	1.5775	-14.2305	0.0282
		ground state	0.1998	17.5493	-0.0075
+1	N3	Q_y	1.8562	3.0528	0.0319
		$\Delta\mu$	1.6564	-14.4965	0.0394
		ground state	-0.3509	8.5923	0.6707
-1	N3	Q_y	1.3706	0.0757	0.6679
		$\Delta\mu$	1.7215	-8.5166	-0.0028

a: The charge is 3.5 Å above the atom.
b: Debyes.
b: Debyes.

Note that the higher order response to the presence of the point charge has caused a relaxation of the electron charge density that is indicated by the altered values of μ_o and μ_{Qy} relative to the unperturbed case reported in Table 2.3. Yet there still remains a net shift of electron density along the y-axis towards ring I in the Q_y transition. Thus, while the point charge modifies the magnitude of the state dipoles, the relative orientations of

the point charge to these dipoles still qualitatively describes the resultant Q_y spectroscopy well, given the magnitudes of charges used in this study.

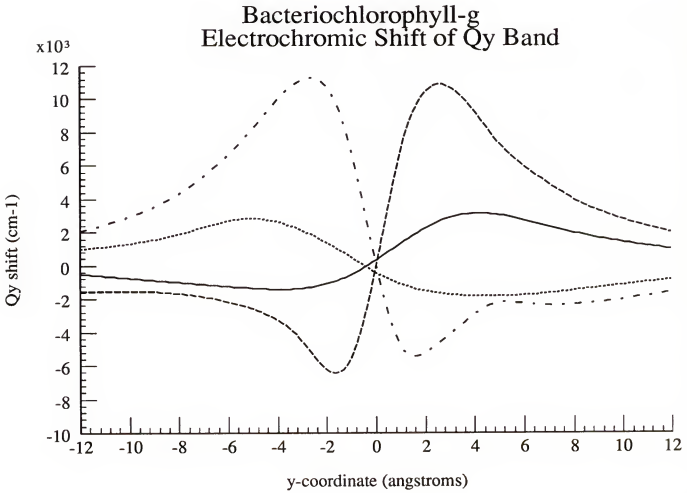

Figure 2.7 Electrochromic shift of Q_y band of bacteriochlorophyll-g (BChlg) in the presence of point charges placed along the molecular y-axis and 3.5 Å above the macrocycle plane (Figure 2.4). The zero y-coordinate is 3.5 Å above the Mg atom with negative y-coordinate values towards ring III and positive y-coordinate values towards ring I. The four lines represent: (solid line) INDO/S-CI with -1.0 a.u. pt. charges (- - -) INDO/S-CI with +1.0 a.u. pt. charges (— — —) pt. charge — pt. dipole interaction with -1.0 a.u. pt. charges, and (—.—.—.) pt. charge — pt. dipole interaction with +1.0 a.u. pt. charges. The electrochromic shift reported is relative to a calculation of the unperturbed BChlg molecule.

In order to more systematically examine the distance and orientation dependance of a point charge on the Q_y transition, a point charge was sequentially placed 3.5 Å above and along the molecular y-axis of BChlg. Figure 2.7 gives a plot of the calculated electrochromic shift along the y-coordinate for this series. A positive y-coordinate is on the ring I side of the molecule while a negative y-coordinate is on the ring III side (Figure 2.4). The distribution of shifts obtained agrees with Figure 2.5. There is both an angular and distance dependance to the electrochromic shift as exhibited by the rising and tailing off of the curve. Also shown is the predicted shift given by a simple point charge-point dipole interaction, eqn. 2.9, as the leading term in a multipole expansion for the classical interaction of a point charge with a charge distribution.

$$\delta E = \frac{q(\Delta\overline{\mu} \cdot \overline{r})}{r^3} \tag{2.9}$$

Here q is the charge of the point charge, r is the distance between the point charge and the origin of the point dipole, and $\Delta\overline{\mu} = \overline{\mu}_{Qy} - \overline{\mu}_o$. The molecular dipole moments were those obtained from the relevant INDO-CI calculation in the presence of each point charge, corrected for the presence of the point charge. While the quantitative behavior of the predicted spectral shifts are overstated by the dipole approximation, the qualitative features are reproduced. The reason for lack of quantitative agreement is, in part, due to the nature of the multipole expansion which is accurate in its truncated form only at distances far from the charge distribution. This criterion is not fulfilled in our calculations where the point charges are routinely placed in van der Waals contact with the molecule. In addition, the quantum chemical dipole formula used (which includes one-center polarization terms) is not completely consistent with the INDO methodology used to calculate the spectra, which includes the point charges only in the diagonal of the Fock matrix (eqn 2.8). It is apparent that the presence of the point charge induces higher multipoles in the molecular electronic distribution of the molecules used in this study. These observations also apply to the other molecules in this study.

The relative magnitude of the calculated δE values is generally BChlg > BChlb > BChla > (P)Chla. Eccles and Honig observed the same relationship for the latter three molecules (examining chlorophyll-a instead of PChla) when they examined the magnitudes of predicted red shifts using a CNDO/S method[49, 50]. We find that the trend applies for both red and blue shifts and is systematically predictable as shown above. We find that the order can be explained by the relative values of the calculated $|\overline{\mu}|$ where BChlg has the largest value and PChla has the smallest. For a given molecule, the differential interaction of the point charge with μ_o and μ_{Qy} is enhanced the more the dipoles differ in magnitude.

Application to the Photosynthetic Reaction Center

The primary charge transfer event in reaction centers of purple bacteria is believed to generate a dimeric BChl cation (P^+) and a BPh anion on the L-branch (BPh^-)[19, 23, 51–53]. Subsequently, the negative charge migrates to the quinone Q_A. P^+ and BPh^- lie within van der Waals contact on opposite sides of a lone accessory BChl "bridging" molecule, $BChl_L$[7, 8, 54–56]. Spectral changes in the red (Q_y) band of the bridge BChls have been observed on picosecond time scales following excitation of the reaction center (RC)[23, 51] and have been attributed to the formation of a BChl anion, [57, 58] (i.e. P^+ $BChl_L^-$ precedes P^+ $BPhl_L^-$) or to electrochromic effects[59, 19, 52]. Other pigments in the RC such as $BChl_M$ and BPh_L, also lie within close proximity of charged species as the charge separation and migration occur. Indeed, shifts in the BPh absorption bands have been observed to accompany quinone reduction[52, 60]. We present below, calculations that examine the electrochromic effects of the charged species P^+, $BChl_L^-$, $BPhl_L^-$, and Q_A^- upon the optical spectra of all the accessory BChls and BPhs in the RC.

Point charges representing P^+, $BChl_L^-$, $BPhl_L^-$ and Q_A^- in bacterial reaction centers were placed at the centroids of the special pair P, $BChl_L$, $BPhl_L$, and between the two oxygens of Q_A using coordinates from the *Rhodopseudomonas viridis* structure. The

calculated shifts induced by these point charges on the optical spectra of the accessory BChls and the BPhs are presented in Tables 2.5 and 2.6.

Table 2.5 Effect of Donor and Acceptor Charges on the Q_y (red) Band of the Bridging BChls of *R. viridis* Reaction Centers.

Bridging BChl	Point charge	Point charge position	Frequency shift of Q_y relative to no charge (cm^{-1})	
L	+1	Center of the $(BChlb)_2$ 3.94, -9.93, 2.54 angs. [a]	1063	blue
L	-1	Center of the $BPhb_L$ -1.41, 5.54, 8.46 angs.[a]	653	blue
L	+1, -1	Cation and anion located as above	1857	blue
L	10 charges of +0.1 a.u. distributed over the 2 Mg and 8N of $(BChlb)_2$		924	blue
L	4 charges of -0.25 a.u. distributed over the 4N of $BPhb_L$		664	blue
L	+, - Cation and anion distributed as above		1709	blue
L	-1	midpt of two O's of Q_A -9.65, 7.47, 19.06 Å	-194	red
L	+1, -1	$(BChlb)_2^+$ and Q_A^-	1063	blue
M	+1	Center of the $(BChlb)_2^+$ 5.20, -9.92, 2.32 angs. [a]	947	blue
M	-1	Midpoint of two O's of Q_A 2.03, -7.18, 29.57 angs. [a]	-34	red
M	+1, -1	$(BChlb)_2^+$ and Q_A	947	blue

a: x, y, and z coordinates of the $(BChl)_2$, $BChl_L$, BPh_L or Q_A relative to the center of the bridging BChl. N1 and N3 of the bridging BChl define the y-axis (Figure2.4).

Table 2.6 Effect of Donor and Acceptor Charges on the Q_y (red) Band of the BPhs of *R. viridis* Reaction Centers.

BPh	Point charge	Point charge position	Frequency shift of Q_y relative to no charge (cm^{-1})	
L	+1	Center of the $(BChlb)_2^+$ 11.48, 12.92, -2.04 angs. [a]	0	
L	-1	Center of the $BChlb_L$ 1.42, 10.03, 1.26 angs. [a]	1825	blue
L	+1, -1	Cation and anion located as above	1356	blue
L	-1	Midpoint of two O's of Q_A -2.69, -9.63, -9.17 angs. [a]	-385	red
M	+1	Center of the $(BChlb)_2^+$ 13.14, 12.44, -0.43 angs. [a]	-390	red
M	-1	Center of the $BChlb_L$ 22.02, 8.87, 5.81 angs. [a]	< 60	blue
M	-1	Center of the $BPhb_L$ 19.38, 2.00, -12.87 angs. [a]	< -40	red
M	-1	Midpoint of two O's of Q_A 15.79, -10.94, -14.79 angs. [a]	< -200	red

a: x, y, and z coordinates of the $(BChl)_2$, $BChl_L$, BPh_L, or Q_A relative to the center of the BPh. N1 and N3 of the Bph define the y-axis.

The positive charge on P^+ and the negative charge on BPh_L^- places these two charges about the bridging $BChl_L$ in an orientation of a positive charge near ring III and a negative charge near ring I. Thus, according to the observations on (B)Chl monomers above, we expect to observe both charges inducing blue shifts in the Q_y band of $BChl_L$. The signs of the shifts follow the pattern observed above and their magnitudes depend

upon both the relative orientation of the charge and its distance from the macrocycle. The calculations indicate that the primary charge separation in a RC should induce a significant electrochromic effect on the optical spectrum of $BChl_L$. Shifts were calculated for a positive charge placed at the donor centroid ($P^+ = BChlb_2^+$) and a negative charge at the $BPhl_L$ center, as well as distributing the point charges over the cores of the donor and primary acceptor (Table 2.5). Individually or together, these charges induce sizeable blue shifts for $BChlb_L$. Oxidation of P to P^+ induces a comparable blue shift for the accessory BChl on the inactive M side. However, $BChl_M$ is sufficiently distant from the pigments on the L side that formation of any L anionic species has little additional effect.

In qualitative agreement with the trends predicted by the calculations, experimental blue shifts of a few hundred wave numbers in the spectra of the bridging BChls have indeed been observed on picosecond time scales, and when the donor is chemically oxidized or the acceptor is reduced under steady state conditions[23, 51]. In addition, P^+ $BPhl_L^-$ induces a larger blue shift on $BChl_L$ than P^+ Q_A^-[61].

Small red shifts are calculated for the influence of P^+ upon BPh_M, and for Q_A^- upon both BPhs (Table 2.6). Experimentally, quinone reduction is indeed accompanied by red shifts in the BPh spectra[52, 60]. The data in Table 2.6 also suggest that if P^+ $BChl_L^-$ preceded P^+ BPh_L^- as a discrete state in the initial charge separation in RCs, then a sizeable blue shift would be expected for the BPh_L prior to its reduction. Subpicosecond measurements have not revealed such an effect in the BPh_L band[23, 51].

The calculations correlate well with observed shift patterns for both the accessory BChls and the BPhs in RCs, supporting an electrochromic origin for these shifts. However, the calculations overestimate the magnitudes of the shifts, because they do not take into account shielding by the protein and ring substituents, or the fact that the charge on the macrocycles is delocalized over the macrocycle[59]. The electrochromic effects would be susceptible to additional modulation if changes in distances or orientations between the chromophores follow electron transfer.

CHAPTER 3
THE ANOMALOUS RED SHIFT

Introduction

The UV/Vis spectroscopy of chlorophylls (Chls) and bacteriochlorophylls (BChls) often differs greatly from *in vitro* to *in vivo*. In particular, the long wavelength transition of bacteriochlorophyll-b (BChlb) in reaction centers (RC) of the photosynthetic bacterium *Rhodopseudomonas viridis* exhibits a large red shift (12500 cm^{-1} (800 nm) *in vitro* and 10416 cm^{-1} (960 nm) *in vivo*) of about 2100 cm^{-1}. If photosynthetically active RCs from these bacteria are treated with detergent and the BChls recovered, a single Q_y absorption maximum characteristic of the *in vitro* absorption maximum is observed. Similar observations are true for the bacteriochlorophyll-a (BChla) containing RCs of the bacterium *Rhodobacter sphaeroides* which exhibits a somewhat smaller *in vitro* to *in vivo* red shift. Contrary, similar large red shifts for the BChl containing antenna proteins (AP) from these bacteria are not observed. Recently, the atomic level X-ray crystal structure of a bacterial RC was published at 3.0 Å resolution and later refined to 2.3 Å resolution [7–9]. Later, the X-ray crystal structure of the RC from *Rb. sphaeroides* was also published [10]. Both RCs contain a pair of BChls closely juxtaposed within van der Waals contact forming a special pair dimer. Figure 3.8 shows the BChlb dimer from *Rps. viridis*. The BChlbs overlap with ring I with the macrocycle planes nearly parallel and separated by about 3.3 Å average distance. The structure for the BChla dimer of *Rb. sphaeroides* is similar with the macrocycle planes separated by about 3.5 Å. These BChl dimers are now known to be the primary electron donor in photosynthetic electron transport in the RCs and are responsible for the anomalously red shifted long

wavelength absorption.

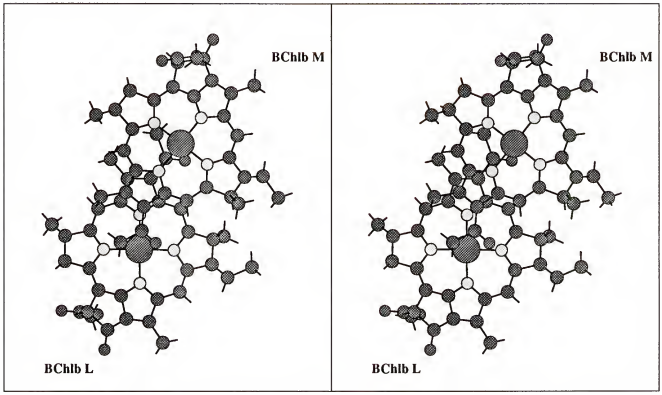

Figure 3.8 Stereo view of bacteriochlophyll-b dimer from *Rps. viridis*. The phytol chains from ring IV have been truncated. The macrocycles are labelled as to their major association with protein subunits L or M.

Norris et al. first proposed in 1971 the existence of a dimer or "special pair" as the primary electron donor in RCs.[17, 62] Their arguments were based on the observation of ESR linewidth narrowing of the cation radical of Chl under conditions where aggregation of the Chls was known to occur. The delocalization of spin density over several Chls was the basis for this experimental observation. Quantifying this line narrowing in terms of the number of Chl monomers involved in the aggregate, they demonstrated that a dimer was consistent with the *in vivo* ESR linewidths for green algae, blue-green algae and some photosynthetic bacteria. Other work, mainly done on Chl containing PSI (P700) of algae and plants, argued that perhaps other perturbations could explain the optical/redox properties of Chls *in vivo*. These include enolization of the ring V keto, ligation of the central Mg atom, electrostatic interactions with charged groups, or the

presence of protonated Schiff base moieties [63–66]. The atomic structure of PSI and PSII from plants and algae is not known, though the successful crystallization of PSI from spinach chloroplasts has recently been reported [6]. Inasmuch as PSI is thought to be evolutionarily related to bacterial RCs, it may be that PSI will contain a special pair dimer of Chl, though this is at present speculative.

Clearly there is something special about the micro-environment the (B)Chls experience in the RC that is different from the AP's, and represents a large change in optical and redox properties relative to *in vitro*. The reasons for this large red shift have been attributed to electrochromic effects from nearby charged or polar amino acids, solvent effects, or simply dimer formation [49, 35, 67].

Coupled Chromophore Models

Theoretical calculations of (B)Chl aggregates are common [68–74]. Even before the report of the crystal structure of bacterial RCs, theoretical methods were employed to ascertain possible conformations of chromophores in RCs [75, 3]. The majority of these studies have been done using the coupled chromophore model which is a phenomenological model for calculating the properties of aggregates [76]. In this model, the zeroth order Hamiltonian for the aggregate consists of the noninteracting local excitations of the constituent monomers.

$$H^0_{\text{aggregate}} = \sum_{i}^{\text{monomers}} H^0_i \tag{3.1}$$

Here H^0_i represents the Hamiltonian for the energy of the local excitations on monomer i. The wavefunction for this Hamiltonian is a simple product wavefunction of the local zeroth order ground state wavefunctions of the monomers.

$$\Psi_{\text{aggregate}} = \prod_{i}^{\text{monomers}} \psi^0_i \tag{3.2}$$

Traditionally, the first order interaction of these local excitations between monomers is introduced with a perturbation correction to the zeroth order Hamiltonian.

$$H_{aggregate} = H^0_{aggregate} + \sum_{A<B}^{monomers} \sum_{B}^{monomers} V_{AB} \tag{3.3}$$

Here V_{AB} represents the electric field interaction between all the local states on monomers A and B. In the basis of local excitations for all monomers, equation 3.3 can be rewritten.

$$H_{aggregate} = \sum_{n}^{N} |n\rangle E_n \langle n| + \sum_{m<n}^{N} \sum_{n}^{N} |n\rangle V_{nm} \langle m| \tag{3.4}$$

The summations are over all the local excitations in the coupled chromophore basis, E_n is the energy of local excitation n, and V_{nm} is the first order interaction between local excitations n and m. For uncharged monomers, the leading term in the perturbation operator, V, will be a dipole-dipole interaction.

$$V = \frac{\mu_1 \cdot \mu_2}{R_{12}^3} - 3\frac{(\mu_1 \cdot R_{12})(R_{12} \cdot \mu_2)}{R_{12}^5} \tag{3.5}$$

Here μ_1 and μ_2 are the moment operators for basis states 1 and 2 respectively on different monomers, and $\mathbf{R_{12}}$ is the vector connecting the center of charge of these monomers. Equation 3.5 represents the leading terms in the interaction of two point dipoles.

With the description of the specific geometry of the special pair in bacterial RCs, there was a greatly renewed effort in attempting to describe the red shift using coupled chromphore theory [77, 78, 33, 72, 79, 75, 80, 74]. Typically the energies and moments of the zeroth order basis states of the monomers were solved using a semi-empirical theory or based upon experimental values for monomers *in vitro*. The results obtained from these studies gave calculated red shifts that were too small, usually being on the order of 300–1000 cm^{-1} compared to the roughly 2100 cm^{-1} *in vitro* to *in vivo* red shift observed for the special pair of *Rps. viridis*. In fact the experimental results could only be reproduced by allowing the zeroth order states to be parameters and adjusting their energies. The justification for this was that there were solvent effects (protein) specific

perturbations from charged or polar amino acid side chains, or effects of secondary protein structure (i.e. dipole moments from α–helices) present that could not be specifically quantified. In reality, one of the problems with some of these calculations was an inadequate basis set over the monomer states. These basis sets usually consisted of local excitations only. In fact, cross excitations or charge transfer (CT) transitions should be included in the coupled chromophore basis set. This has been known for some time [81, 82] and should be obvious based on simple physical arguments. Typically the energy of a local Q_y state (the value of E_n, n=Q_y, in equation 3.4) will be about 12500 cm^{-1} for BChlb. We can approximate the energy of a CT transition from one chromophore to another by

$$E_{CT} \approx I_A - A_B - \frac{1}{R_{AB}} \tag{3.6}$$

Here I_A is the ionization potential of chromophore A, A_B is the electron affinity of chromophore B, and $\frac{1}{R_{AB}}$ is the electrostatic interaction of the resulting ionic pair. For bacteriochlorin derivatives, typical values of I_A and A_B are about 6 eV and 1 eV [3] respectively. If the center of charge of the two chromophores is 5 Å apart, then equation 3.6 gives a value of about 16000 cm^{-1}, well within an energy range accessible to interact with the local Q_y states. Warshel and Parson realized this and published an elegant study of a modified coupled chromophore approach that took account not only of the CT excitations between the special pair monomers but the local excitations and CT excitations with the other BChl and BPh chromophores present in the RC of *Rps. viridis* [77, 78]. In their study they observed that CT excitations between the monomers of the special pair contributed to the lowest energy excitation of the RC. Their results exhibited a further red-shifting and lessing of the intensity of this absorption band. However, to obtain results that were consistent with UV/Vis, optical activity (CD) and linear dichroism (LD) they still had to treat the local zeroth order states as adjustable parameters (though not as severely as previous studies) and arbitrarily adjust the CT transitions. While they adequately described the lowest energy state of the RC as being composed of mainly the

lower exciton state ($P_{(-)}$) of the BChlb dimer, their placement of the upper exciton state ($P_{(+)}$) at about 800 nm conflicts with experiment which places this state at about 850 nm Furthermore their somewhat arbitrary adjustment of the CT states between the monomers of the BChlb dimer presumed a direction for the asymmetric charge redistribution in the dimer for the lowest excited state. This charge asymmetry in the dimer excited states (ascertained from Stark effect data [83]) is thought to be a precursor to determining the vectorial electron transport along only one of the chromophore branches of the RC. This is not well understood and remains controversial. Clearly there was a need for a somewhat more rigorous and less biased treatment of the excited states of the BChlb dimer in bacterial reaction centers.

Results and Discussion

The properties of (B)Chl aggregates can be described in a supermolecule fashion as well. Thus we obtain a description of the ground and excited state properties of the aggregate in terms of SCF molecular orbitals delocalized over the whole complex. Although the simple physical picture generated by coupled chromophore models is apparently lost, we can obtain a less biased description of the electronic structure and properties of the excited states. Also, as the chromophores get closer together and interact more strongly, the coupled chromophore model becomes inadequate. Indeed, *ab initio* studies have shown that Mg porphyrin-porphine dimers that were within van der Waals distances were better described as supermolecules[71]. The coupled chromophore model is still a useful description for (B)Chl dimers. We show in Chapter 4 that a coupled chromophore description can be projected out of a supermolecule SCF MO description of bacteriochlorin dimers and demonstrate regions of validity for the coupled chromophore model.

Using the semi-empirical INDO/S method we calculated the UV/Vis spectra for the BChlb dimer from the RC of *Rps. viridis* first using the 3.0 Å resolution coordinates

(results published in [67]) and more recently with the 2.3 Å resolved coordinates. Results presented below are from the latter. The structure of the BChlb dimer is shown in Figure 3.8. The phytol chains on ring IV have been truncated. The macrocycles are cofacial with an overlapping of ring I. The planes of the macrocycles are nearly parallel and are rotated roughly 15° relative to one another about an axes passing through their respective Mg atoms and perpendicular to the macrocycle planes. The N_{III} —> N_I axis (defined as the molecular y-axis) for each macrocycle are then roughly antiparallel. The fifth coordinate position of each Mg atom is occupied by the imidazole ring from adjacent histidine amino acid residues (not shown). Also there are some hydrogen bonding amino acid residues interacting with the BChlb dimer (not shown). The effects of these moieties will be addressed in Chapter 5. Furthermore the constituent BChlb monomers in the dimer are not structurally the same. The M BChlb has its macrocycle ring slightly puckered.

The INDO/S CI calculation of the excited states of the BChlb dimer utilized all single electron promotions from the 28 highest occupied MOs into the 28 lowest unoccupied MOs. The results for this calculation as well as an equivalent calculation of the constituent monomers are shown in Table 3.7.

Table 3.7 INDO/S Results for the Low Energy State(s) of the BChlb Dimer and its Constituent Monomers

	Q_y ($P_{(-)}$ [a])		$P_{(+)}$ [b]	
	Energy (cm^{-1})	Oscillator Strength	Energy (cm^{-1})	Oscillator Strength
BChlb Dimer	10786	0.986	12345	0.136
BChlb M [c]	12789	0.571	NA[d]	NA
BChlb L	12484	0.649	NA	NA

a: Q_y state for monomer BChlb. The lowest excited state of the BChlb dimer is labelled $P_{(-)}$ which represents the lower exciton band of the dimer.

b: $P_{(+)}$ represents the upper exciton band of the dimer.

c: The monomers are labelled as to their major association with either the L- or M-protein subunit in the reaction center (Figure 1.3).

d: Not Applicable to BChlb monomers.

The long wavelength absorption maximum for the *Rps. viridis* reaction center *in vivo* is about 10400 cm^{-1} (960 nm) while the BChlb monomer absorbs at about 12500 cm^{-1} (800 nm). The BChlb M monomer is known to have a macrocycle that is puckered relative to the BChlb L monomer. Thus we observe the two monomer's Q_y transitions split by about 300 cm^{-1}. We calculate an average BChlb monomer Q_y absorption maximum of 12636.5 cm^{-1} and the BChlb dimer $P_{(-)}$ band at 10786 cm^{-1}. The calculated red shift is 1850 cm^{-1} compared with about 2100 cm^{-1} experimental value. The $P_{(-)}$ and $P_{(+)}$ bands are labelled as the lower and upper exciton bands of the BChlb dimer respectively. This labeling comes from coupled chromophore studies [77, 78]. In Chapters 4 and 5 we demonstrate that the lowest two excited states for the dimer (calculated with a supermolecule approach using INDO/S) are dominated by the lower and upper exciton states of the constituent monomers. Experimentally, the $P_{(+)}$ band occurs at 11764 cm^{-1} (850 nm) for *Rps. viridis*. Our INDO/S calculations place this band at 12345 cm^{-1}. The exciton splitting between $P_{(-)}$ and $P_{(+)}$ is 1724 cm^{-1} experimentally, compared to our calculated value of 1559 cm^{-1}. While the nearby amino acids and other chromophores of the RC do exert effects on the BChlb dimer, we observe that the majority of the *in vitro* to *in vivo* red shift can be explained simply on the basis of formation of the dimer alone. We observe charge asymmetry in the calculated excited states of the BChlb dimer (Chapter 5). These charge asymmetries can be thought of as coming from the unbalanced cross CT excitations from the coupled chromophore model. However, unlike the phenomenological coupled chromophore models, we do not arbitrarily adjust the placement of this CT character. These effects are included in the supermolecule approach in a natural fashion that is more indicative of the BChlb dimer's micro-environment in the protein.

In view of the function of the RC, one can argue *post hoc* that it makes sense for the RC to have the optical transition of lowest energy. The AP's, which have a long wavelength absorption of higher energy than the RC, excitonically transfer energy to the RC where the RCs long wavelength transition serves to "trap" this energy and use it in

the initial charge separation steps. It is appealing to speculate that (B)Chl dimers are a universal structure for these phototraps. This seems to be the case for photosynthetic bacteria. However the experimental evidence for green plants (which contain Chl) seems to suggest that monomeric Chls may be present instead of closely interacting dimers. The elucidation of the atomic structure of the recently crystalized PSI should prove interesting [6].

When the RC coordinates for *Rps. viridis* were first published it was apparent to us that a simple coupled chromophore model was inappropriate for describing the BChlb dimer. Although a coupled chromophore picture can be projected out of the supermolecule wavefunction (Chapter 4) the coupled chromophore model alone is incapable of explaining the anomalous red shift. Formation of the dimer by itself appears to be sufficient to induce a large *in vitro* to *in vivo* red shift. This observation would assure that the BChlb dimer possessed the electronic absorption of lowest energy required for it to be an effective phototrap.

CHAPTER 4
ELECTRONIC STRUCTURE OF BACTERIOCHLOROPHYLL DIMERS: BACTERIOCHLORIN MODELS

Introduction

An explanation of the electron transport process must involve interactions of all six chromophores in addition to the other moieties present in the reaction center. However, the BChlb special pair acts as the primary electron donor and thus plays a pivotal role in the initial light driven charge separation. An examination of the geometry of the BChlb special pair reveals that it is not exactly symmetric, and theoretical calculations show that there are asymmetries in the electronically excited state surfaces of this dimer [84, 31, 85]. The sensitivity of the lowest energy, or Qy, band of the reaction center of both *Rps. viridis* and *Rhodobacter sphaeroides* to external electric fields (Stark effect) is taken as an indication of charge separation occurring within this state [83, 86–88]. This initial charge separation must surely play a role in determining the vectorial electron transport along the L-branch. Furthermore, a choice between the various models proposed for the electron transport mechanism will in part require an adequate description of the electronic structure of the excited state surfaces of the bacteriochlorophyll dimer [31, 24, 28, 29]. Theoretical calculations of Plato et al. have shown a partial charge separation in the lowest excited state from the L to the M BChlb of the special pair of *Rps. viridis* using an INDO model Hamiltonian [84]. However, these results appear to be sensitive to small changes in the geometry of the special pair. Other theoretical studies of reaction centers have been reported recently[33, 77, 78, 74, 73]. Most of these involve the use of exciton based theories of interacting monomers. While these approaches have provided valuable

insights of the dimer and the full reaction center, the models have generally required arbitrary fitting of the monomer wavefunctions to reproduce the photophysics of the reaction center. Indeed, for the lowest electronic excited state of the *Rps. viridis* reaction center, Parson and Warshel predict a partial separation of charge from the M to the L BChlb of the special pair which resulted from fitting the two inter-chromophore charge transfer (CT) energies to reproduce linear dichroism and CD spectra [78]. Recently, a study of the reaction center of *Rps. viridis* employing both an INDO model Hamiltonian for the SCF and an exciton model of the excited states showed an L to M BChlb net charge separation in the first excited state [33]. A description of the electronic structure of the excited states is lacking in these models. How the first excited state of the special pair acquires net CT character is an important and as yet unresolved question. Clearly, a detailed quantum chemical study of the nature of the low lying excited states of the special pair and their sensitivity to fields, geometric perturbations, and the protein environment is required.

We report here a study of model dimers composed of magnesium bacteriochlorins (MGBC) that probes the effects of geometric configurations on the electronic excited states of the dimers in the absence and presence of static electric fields. We extract a physical picture of the electronic states in an *a priori* way. The results describe the consequences of bringing two chromophores together on optical spectra and on excitonic and charge transfer interactions. Furthermore, they provide insights into the factors that determine the properties of the special pairs *in vivo*, and may also be relevant to the properties of BChl antenna proteins that also contain BChl aggregates. A report of these results has been presented.[89, 90]

Intermolecular Spacing and Electric Fields

The UV/visible spectroscopy of porphyrins and their derivatives may be understood in a simple fashion in terms of Gouterman's 4-orbital model.[46] For porphyrins with

D4h symmetry, the four molecular orbitals (MOs) of this model are the two Highest Occupied MOs (HOMOs) which have symmetry a_{1u} and a_{2u} and the Lowest Unoccupied pair of MOs (LUMOs) having e_g symmetry. Configurations involving single excitations from the HOMOs into the LUMOs reproduce the optical spectra correctly only when the four possible configurations are allowed to undergo configuration interaction. These final CI states are labelled Qy, Qx, By, and Bx. Due to configuration mixing in the CI, the Soret, or B bands contain nearly all the intensity while the Q bands are weak. In a bacteriochlorin, the symmetry of the macrocycle is reduced from D4h to D2h by saturation of the exocyclic double bonds of pyrrole rings II and IV, the a_{1u} MO is 'pushed' up in energy, and the degeneracy of the e_g MOs is removed (while the D4h symmetry labels no longer apply, the D4h origin of the bacteriochlorin MOs is still apparent and it is traditional to retain these orbital labels). The consequences are that the two y-polarized configurations are no longer nearly degenerate. The Qy band is red-shifted and of greater intensity while the By band is blue-shifted and has lost intensity relative to porphyrin. The x-polarized excitations are, however, still nearly degenerate as in the porphyrin case and the resulting Qx band is still weak. The 4-orbital model explains the low energy photophysics of porphyrins quite well, even though the contributions of more extensive CI to the B bands are known to be important [91]. The applicability of the 4-orbital model and its extension to dimers of reduced porphyrins will be central to the arguments contained in this paper, although the actual calculations are more complex.

Exciton theory has been applied extensively to the study of complexes of porphyrin derivatives [77, 78, 74, 73]. In this coupled-chromophore model, the local excitations of the monomers are coupled via interaction matrix elements of the Hamiltonian:

$$H = \sum_{n=1}^{N} |n> E_n <n| \quad + \sum_{m \neq n=1}^{N} |n> V(n,m) <m| \tag{4.1}$$

Here the summations are over the basis of the local excitations of the monomers. E_n represent the energies of the singlet states of the monomers and the V(n,m) are the interactions between these states [74]. The summations in equation 4.1 include charge

transfer excitations between the constituent monomers. By solving the secular equation for this interaction of the monomer states, an approximation to the dimer spectroscopy is obtained. This description is appealing in its ability to describe the dimer states in terms of a simple picture. The results of this approach, while correct in their description of trends, in practice usually require significant rescaling of the monomer energies to correctly reproduce the properties of the complex, particularly if the monomers interact strongly and behave as a supermolecule. Alternatively, one can directly calculate the dimer spectra using traditional molecular orbital methods. Although the results are less biased because they do not require rescaling parameters, the physical picture of the coupled-chromophore model is not obvious.

When two Mg-bacteriochlorins (MGBC) are juxtaposed with their macrocycle planes parallel, the 4–orbitals of Gouterman's model become 8–orbitals in the dimer, as shown in Figure 4.9.

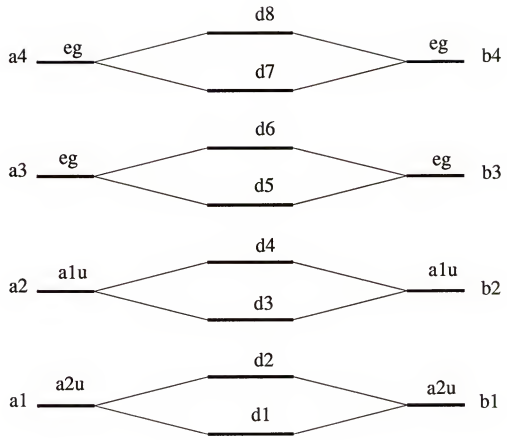

Figure 4.9 Molecular orbitals of a Mg-bacteriochlorin dimer and the monomer constituents. The monomer labels are those for D4h symmetry and are retained for convenience. The dimer labels are described in the text. For a neutral closed shell calculation (RHF) dimer, MOs 1–4 are doubly occupied and MOs 5–8 are unoccupied.

The monomer MOs are labelled "a" and "b" with the MOs numbered in increasing energy. The dimer MOs are numbered d1–d8 with d1–d4 doubly occupied and d5–d8 unoccupied. In the dimer, there are 16 possible singly excited configurations within this 8-orbital manifold in contrast to the four delineated for the monomer. If the dimer MOs are 'derived' from specific monomer MOs (ie., dimer MOs d1 and d2 arise from an interaction of monomer MOs a1 and b1) then each of the monomer CI states will be

related to four CI states in the dimer. Thus, there will be four dimer spectroscopic states with 'Qy origins', which we label as Qy1, Qy2, Qy3, and Qy4 in increasing order of energy and collectively referred to as the Qy states.

The dimer MOs can be expressed as expansions of the monomer MOs.

$$\psi_i^{dimer} = \sum_{A}^{monomers} \sum_{\mu \in A}^{MO's} C_{i\mu} \ \psi_\mu^{monomer} \tag{4.2}$$

When the dimer does not behave as a true supermolecule, it is easy to extract a coupled-chromophore picture of the localized MOs using this expansion. We consider now the case where the sums in equation 4.2 are limited only to the near degenerate monomer MOs as pictured in Figure 4.9. Thus each dimer MO is a linear combination of two monomer MOs. The determinants of the spin adapted dimer configurations can then be re-expressed in terms of these monomer MOs. Equation 4.3 demonstrates this for one determinant from the $\Psi_{d_4}^{d_5}$ spin adapted configuration (MO labelling as in Figure 4.9)

$$\begin{aligned} \Psi_{d_4}^{d_5} &= |\ldots d_1\overline{d_1}d_2\overline{d_2}d_3\overline{d_3}d_4\overline{d_5}| \\ &= |\ldots (b_1 - a_1)\overline{(b_1 - a_1)} \ldots (-b_2 - a_2)\overline{(b_3 - a_3)}| \end{aligned} \tag{4.3}$$

Here the bars above an orbital designate beta spin. When this re-expressed dimer determinant is simplified, a linear combination of determinants is obtained in which each determinant involves only monomer excitations. In this fashion, each single excited configuration from the dimer is expressed in terms of one electron monomer MO promotions rather than dimer MO promotions. Two types of monomer MO promotions arise naturally from this treatment: local excitations (ie., a2–>a3, b2–>b3) referred to as excitonic (EX) and cross excitations (ie., a2–>b3, b2–>a3) referred to as charge-transfer (CT). States that exhibit balanced CT contributions, and thus have no net charge separation, are referred to as charge-resonance (CR) states. In geometric configurations where the monomers interact strongly as to greatly perturb the monomer character of the MOs this type of analysis is of limited utility. In these cases the first order coupled-chromophore model is inapplicable and a supermolecule approach is better. In the present

analysis, we examine the regions for which the coupled-chromophore model is valid and examine the electronic structure of the dimer in that domain. We are able to clearly identify CR and EX excited states and describe their monomer character.

We initially examine the dimer of Mg-Bacteriochlorin (DMGBC) shown in Figure 4.10. The monomers are positioned with the unsaturated rings overlapped. The macrocycle planes are parallel to the x-y plane with the positive z-axis out of the plane of the figure. The Mg atoms are in the plane of their respective macrocycles. In this configuration, the DMGBC dimer has a center of inversion and a C2 axis of rotation (parallel to the x-axis). The macrocycle rings were separated by 5.0 Å as defined by the plane of the four pyrrole nitrogens of each monomer. The 16 possible singly excited configurations within the 8–orbital manifold of this dimer are distinguished by being either x or y-polarized Table 4.8

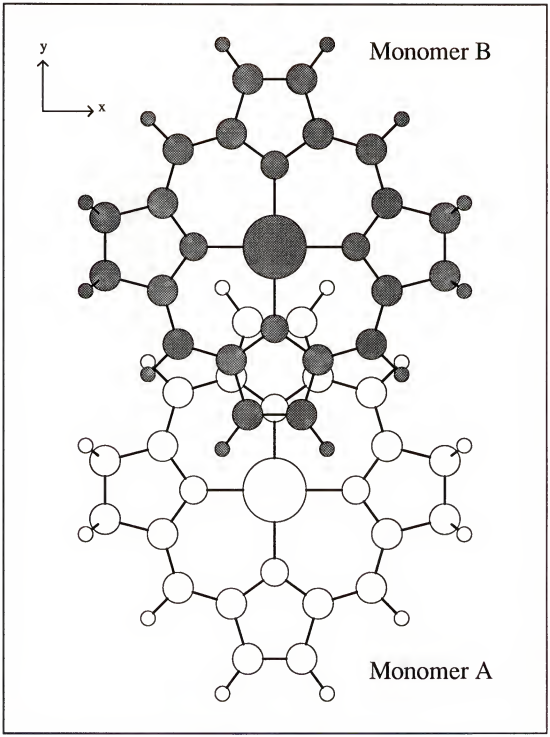

Figure 4.10 Configuration of the Mg-bacteriochlorin dimer at 5.0 Å separation. Monomers are labelled A and B with the latter closer to the viewer.

Table 4.8 DMGBC 5.0 Å Separation. Single excited configurations from the 8–orbital manifold

Configuration	Polarization	Symmetry
d4 -> d5	y	u
d3 -> d6	y	u
d4 -> d6	y	g
d3 -> d5	y	g
d2 -> d7	y	u
d1 -> d8	y	u
d2 -> d8	y	g
d1 -> d7	y	g
d4 -> d7	x	g
d3 -> d8	x	g
d4 -> d8	x	u
d3 -> d7	x	u
d2 -> d5	x	g
d1 -> d6	x	g
d2 -> d6	x	u
d1 -> d5	x	u

with the x and y directions given in Figure 4.10. The results of an INDO/S calculation of this dimer show the symmetry of the monomer MOs contributing to the DMGBC MOs as d1,d2 a_{2u}; d3,d4 a_{1u}; and d5–d8 e_g (Figure 4.9). Furthermore, due to the inversion center, these dimer MOs can be labelled as symmetric (gerade, g) or antisymmetric (ungerade, u) linear combinations of the monomer MOs. A CI was performed that included the lowest 144 singly excited configurations from the INDO/S reference ground state with care being taken not to split any near degeneracies in the dimer MOs. The resulting CI coefficients for the Qy states were almost entirely composed of excitations within the 8–orbital manifold (> 99%). For later analysis, these coefficients were renormalized within the 8–orbital manifold and the results for the Qy states are shown in Table 4.9.

Table 4.9 DMGBC 5.0 Å separation. CI coefficients of the Qy states.

Qy-State	Qy1	Qy2	Qy3	Qy4
Energy cm-1	13081.7	13174.5	16936.3	16936.5
Oscil. Str.	1.2628	0	0	0
Excitation	Exciton	Exciton	CR[1]	CR
d4 -> d5	0.6711	0	0	0.7028
d3 -> d6	-0.6617	0	0	0.7114
d4 -> d6	0	-0.6656	-0.7063	0
d3 -> d5	0	0.6639	-0.7079	0
d2 -> d7	-0.2376	0	0	0.0019
d1 -> d8	-0.2351	0	0	0.0019
d2 -> d8	0	0.2419	-0.0004	0
d1 -> d7	0	0.2401	-0.0004	0

1. Charge resonance

Of the y-polarized single excited configurations, four are of gerade and four are of ungerade symmetry due to the center of inversion Table 4.8. Thus the Qy states are further divided into two symmetry allowed and two symmetry forbidden transitions. In Table 4.9, we observe CI states Qy1 and Qy4 composed of ungerade configurations (symmetry allowed) and states Qy2 and Qy3 composed of gerade configurations (symmetry forbidden). Of the symmetry allowed transitions, Qy4 has zero calculated oscillator strength due to phasing of the configuration mixing. The reason for this is that the d4–>d5 and d3–>d6 configurations are nearly degenerate and have a near equal transition dipole and the same is true for the d2–>d7 and d1–>d8 configurations when the macrocycles are separated by 5.0 Å. These transition dipoles reinforce for Qy1 and therefore Qy1 contains all the intensity from the CI of these four configurations; these transition dipoles cancel for Qy4. We show later that Qy1 is composed almost entirely of EX configurations that are localized on each monomer while Qy4 is a CR state composed almost entirely of balanced cross excitations from one monomer to the other. Compared to an INDO/S

calculation of an MGBC monomer, with equivalent CI, the allowed dimer Qy transition is red-shifted from the monomer Qy transition by 35.6 cm^{-1} and shows nearly twice the calculated oscillator strength of the monomer. This result is expected for MGBC monomers spaced far enough apart to behave to first order as two weakly interacting monomers rather than a supermolecule. The Qx states are also divided into two symmetry allowed and two symmetry forbidden transitions (data not shown). The symmetry allowed transitions Qx1, and Qx4 have calculated oscillator strengths of 0.0063 and 0.0 respectively. As in the monomer, Qx1 is weakly allowed. The x-polarized configurations in the 8-orbital manifold come from excitations from d1,d2 –> d5,d6 and d3,d4 –> d7,d8 (Figure 4.9). Since these configurations are all nearly degenerate, the phasing in the CI will place most of the x-polarized intensity in the B-bands as it does in the monomer. Note that the y-polarized configurations arising from d3,d4 –> d5,d6 excitations are quite different in energy from those of the d1,d2 –> d7,d8 excitations. This results in the Qy states having a much larger calculated oscillator strength than the Qx states. Figure 4.11 shows the INDO/S calculated spectra of DMGBC at 5.0 Å separation up to 45,000 cm^{-1}.

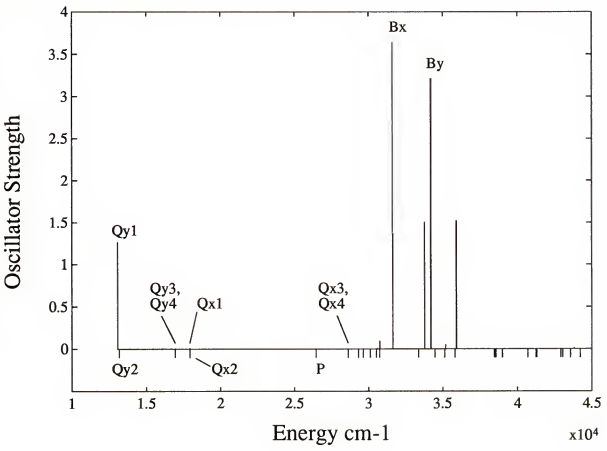

Figure 4.11 INDO/S spectrum of the Mg-bacteriochlorin dimer at 5.0 Å separation. The calculation includes the lowest 144 single excited configurations from the SCF ground state. The negative ticks indicate calculated transitions with zero oscillator strength.

The negative ticks represent transitions of zero calculated oscillator strength. The four transitions of the Qy and Qx states are labelled. The two degenerate bands labelled 'P' that lie to the red of Qx3, Qx4 are x-polarized and derived from excitations from d3,d4 –> d9,d10. Note that d9 and d10 are not part of the 8–orbital manifold in Figure 4.9. The spectrum for the Bx and By states is complicated by mixing with other nearby excited configurations and thus we label only the two strong Bx and By transitions. An even simpler model incorporating a CI of only the 16 configurations from the 8-orbital

manifold gave essentially no change in the behavior of the Qy and Qx bands and greatly simplified the high energy spectra of the Bx and By bands. However, a limited CI of this nature, while modeling the low energy spectrum adequately, is inadequate in describing the high energy region. This is due in part to the high density of states in the UV region and the possibility of contributions from multiply excited configurations. Our subsequent analyses thus incorporate the larger single excited CI, as described in the Methods. For the remainder of this paper we will limit our examination to the low energy transitions of the Qy and Qx states, the states of greatest interest, and those that are generally easy to relate to the coupled-chromophore model. These are also the states that are thought to be photochemically active. We will emphasize the description of the Qy states since these are of the lowest energy and contain most of the oscillator strength. Where applicable, comparisons with the Qx states will be made.

For the case of 5.0 Å separation, the coefficients of the Linear Combination of monomer MO (LCMO) contribution to each dimer MO were seen to be $\pm\frac{1}{\sqrt{2}}$. Table 4.10 lists the symmetry of these LCMOs for the eight dimer orbitals of Figure 4.9.

Table 4.10 DMGBC 5.0 Å separation. LCMO description of the 8–orbital manifold

Dimer MO	Monomer-a	Monomer-b	Symmetry
d1	-a1[1]	b1	ungerade
d2	a1	b1	gerade
d3	-a2	b2	ungerade
d4	-a2	-b2	gerade
d5	-a3	b3	ungerade
d6	a3	b3	gerade
d7	a4	-b4	ungerade
d8	-a4	-b4	gerade

1. Each monomer MO contributes with the same absolute value coefficient of $\pm\frac{1}{\sqrt{2}}$ (see text).

We re-expressed the spin adapted determinants of all the single excited configurations from the 8–orbital manifold in terms of these LCMOs. Table 4.11 summarizes this for the four Qy states examined.

Table 4.11 DMGBC 5.0 Å separation. LCMO of y-polarized configurations.

	Dimer Y-polarized Single Excited Configurations							
Monomer Basis	d4->d5	d3->d6	d4->d6	d3->d5	d2->d7	d1->d8	d2->d8	d1->d7
a2->a3	0.5	-0.5	-0.5	0.5				
b2->b3	-0.5	0.5	-0.5	0.5		This block 0.0		
a2->b3	-0.5	-0.5	-0.5	-0.5				
b2->a3	0.5	0.5	-0.5	-0.5				
a1->a4					0.5	0.5	-0.5	-0.5
b1->b4		This block 0.0			-0.5	-0.5	-0.5	-0.5
a1->b4					-0.5	0.5	-0.5	0.5
b1->a4					0.5	-0.5	-0.5	0.5

The columns of Table 4.11 are the single determinant configurations for the dimer. The rows are the basis of monomer determinants. Due to the symmetry of the dimer, all single excited configurations are composed of equal contributions of monomer EX and CT excitations where only the phasing is different (Table 4.11). By allowing these states to undergo configuration mixing, we re-express the INDO/S CI results in terms of the monomer MO excitations by transforming the y-polarized CI vectors from Table 4.9 in terms of the LCMO coefficients in Table 4.11.

$$\Psi_{\mathrm{LCMO}} = \Psi_{\mathrm{Dimer}}\mathbf{C} \tag{4.4}$$

The columns of matrix C are the rows of LCMO coefficients from Table 4.11, the rows of Ψ_{Dimer} are the CI vectors from Table 4.9. The resulting transformed vectors, Ψ_{LCMO} are shown in Table 4.12.

Table 4.12 DMGBC 5.0 Å separation. LCMO of Qy states.

Qy-State	Qy1	Qy2	Qy3	Qy4
energy cm-1	13081.7	13174.5	16936.3	16936.5
osc. strength	1.2628	0	0	0
Excitation	Exciton	Exciton	CR[1]	CR
a2 -> a3	0.6664	0.6648	-0.0008	-0.0043
b2 -> b3	-0.6664	0.6648	-0.0008	0.0043
a2 -> b3	-0.0047	0.0008	0.7071	-0.7071
b2 -> a3	0.0047	0.0008	0.7071	0.7071
a1 -> a4	-0.2364	-0.2410	0.0004	0.0019
b1 -> b4	0.2364	-0.2410	0.0004	-0.0019
a1 -> b4	0.0012	-0.0009	0.0000	0.0000
b1 -> a4	-0.0012	-0.0009	0.0000	0.0000

1. Charge resonance.

Qy1 and Qy2 are composed almost entirely of EX transitions (a2–>a3, b2–>b3, a1–>a4, b1–>b4) while Qy3 and Qy4 are CR states composed almost entirely of CT transitions (a2–>b3, b2–>a3). Due to the symmetry of this dimer geometry, the CR states Qy3 and Qy4 exhibit no net charge separation. The ordering of the energies of these four states is reasonable since the CT configurations that make up Qy3 and Qy4 are expected to be higher in energy than the EX configurations that make up Qy1 and Qy2. An analysis of the Qx states gave results similar to the Qy states (data not shown): Qx1 and Qx2 were EX states while Qx3 and Qx4 were CR states.

We next imposed an electric $\boldsymbol{E}$ field of 10^{-6} au. along the z-axis which is perpendicular to the planes of the macrocycles (Figure 4.10) (1.0 au. = 5.1419 x 10^{11}V/m). The orientation of this field places the positive plate near monomer-A. Table 4.13 shows the INDO/S CI resulting from this calculation for the Qy states.

Table 4.13 DMGBC 5.0 Å separation. CI coefficients of Qy states in presence of 10^{-6} au. $\boldsymbol{E}_z$

Qy-State	Qy1	Qy2	Qy3	Qy4
energy cm-1	13081.8	13174.5	16934.3	16938.4
osc. strength	1.2628	0	0	0
Excitation	Exciton	Exciton	CR[1]	CR
d4 -> d5	-0.6695	-0.0094	-0.5200	-0.4752
d3 -> d6	0.6601	-0.0090	-0.4544	-0.5494
d4 -> d6	-0.0467	0.6655	0.5041	-0.4925
d3 -> d5	-0.0463	-0.6639	0.5186	-0.4793
d2 -> d7	-0.2374	-0.0084	0.0014	0.0014
d1 -> d8	0.2349	-0.0082	-0.0013	-0.0014
d2 -> d8	0.0104	-0.2418	0.0003	-0.0003
d1 -> d7	0.0102	0.2400	-0.0003	0.0002

1. Charge resonance.

The $\boldsymbol{E}_z$ field removes the center of inversion and C2 axis symmetry elements from the dimer and allows all the y-polarized transitions to mix in the CI (compare Tables 4.9 and 4.13). The x and y polarized configurations still do not mix since the y-z plane forms a symmetry plane. The calculated oscillator strengths are unchanged by the presence of the $\boldsymbol{E}_z$ field and the transition energies are altered for the Qy3 and Qy4 states by only about -2 cm^{-1} and 2 cm^{-1} respectively. While there appear to be small changes to the CI vectors of Qy1 and Qy2, we observe that states Qy3 and Qy4 have changed significantly. Using first order perturbation theory we can express the nature and extent of this configuration mixing. Equations 4.5–4.7 show the $\boldsymbol{E}_z$ perturbed CI vectors (Table 4.13) expressed as a first order mixing of the unperturbed CI vectors (Table 4.9).

$$\Psi_n = \Psi_n^o + \sum_{m \neq n} \Psi_m^o U_{mn} \tag{4.5}$$

$$\mathbf{C}' = \mathbf{C}^o \mathbf{U} \tag{4.6}$$

$$U = (C^{o})^{\dagger} C' \tag{4.7}$$

Here Ψ_n is a perturbed CI vector and Ψ_n^o is its corresponding unperturbed vector. Equation 4.6 is the matrix representation of equation 4.5. The mixing of the zeroth order states is represented by the matrix elements of U. The results for matrix U for this case are summarized in Table 4.14.

Table 4.14 DMGBC 5 Å Separation. Qy States 1st Order Perturbation Configuration Mixing With 10^{-6} au. E_z Field.

	Perturbed CI Vectors			
Basis[1]	Qy1	Qy2	Qy3	Qy4
Qy1°	-0.9976	-0.0010	-0.0505	0.0480
Qy2°	0.0010	-0.9999	0.0094	0.0102
Qy3°	0.0697	0.0003	-0.7232	0.6871
Qy4°	0.0000	-0.0138	-0.6887	-0.7249

1. Basis of unperturbed CI vectors in the absence of any E field.

The large interaction between Qy3 and Qy4 is expected since the first-order perturbation correction to the wavefunction is inversely dependent upon the energy difference between the zeroth order states that mix. To demonstrate that this is largely a CI effect at this field strength, we show in Table 4.15 the dimer MOs expressed as LCMOs.

Table 4.15 DMGBC 5 Å Separation. Monomer Contributions to Dimer 8-Orbital Manifold With 10^{-6} au. E_z Field.

Dimer MO	Monomer-a	Monomer-b
d1	0.7104 a1	-0.7038 b1
d2	-0.7038 a1	-0.7104 b1
d3	0.7268 a2	-0.6870 b2
d4	0.6870 a2	0.7268 b2
d5	-0.7360 a3	0.6770 b3
d6	0.6770 a3	0.7360 b3
d7	-0.7341 a4	0.6790 b4
d8	-0.6790 a4	-0.7341 b4

The dimer MOs have split only slightly in terms of their LCMO composition and each monomer MO retains its unperturbed symmetry to a large extent. Utilizing the LCMO coefficients from Table 4.15, we re-express the spin-adapted configurations from the 8–orbital manifold in terms of their monomer MO contribution (eqn. 4.3) and show the resulting interpretation of the CI (eqn. 4.4) in Table 4.16.

Table 4.16 DMGBC 5 Å Separation. LCMO of Qy States With 10^{-6} au. E_z Field.

Qy-State	Qy1	Qy2	Qy3	Qy4
energy cm-1	13081.8	13174.5	16934.3	16938.4
osc. strength	1.2628	0	0	0
Excitation	Exciton	Exciton	CR[1]	CR
a2->a3	0.6663	0.6649	-0.0037	-0.0027
b2->b3	-0.6664	0.6666	0.0008	0.0048
a2->b3	-0.0046	0.0006	0.0251	-0.9996
b2->a3	0.0048	0.0010	0.9996	0.0250
a1->a4	-0.2363	-0.2411	0.0017	0.0012
b1->b4	0.2364	-0.2410	-0.0010	-0.0017
a1->b4	0.0013	-0.0009	0.0000	0.0000
b1->a4	-0.0012	-0.0009	0.0001	0.0000

1. Charge resonance.

States Qy1 and Qy2 remain largely EX in character as in Table 4.12. However, Qy3 and Qy4 are each dominated by one CT excitation. State Qy3 is predominately a b2–>a3 cross-excitation and Qy4 is an a2–>b3 cross-excitation. The energy ordering of these two states is reasonable as this E_z field will favor a negative charge on monomer-A. The INDO/S calculated state dipole moments for the Qy states in the presence of this E_z field are shown in Table 4.17.

Table 4.17 DMGBC 5 Å Separation. State Dipole Moments[1] of Qy States With 10^{-6} au. E_z Field.

	μ_x	μ_y	μ_z
Ψ_o	0	0	0.0003
Qy1	0	-0.0004	0.0004
Qy2	0	0.0003	0.0003
Qy3	0	27.6752	23.9845
Qy4	0	-27.6752	-23.9839

1. Units are debyes.

The unbalanced CT character of Qy3 and Qy4 is evident from their large calculated dipole moments while Qy1 and Qy2 show no appreciable charge separation. In Figure 4.12 we show the calculated transition energies of the Qy states as the strength of the E_z field is varied from 0.0 to 10^{-3} au. in strength.

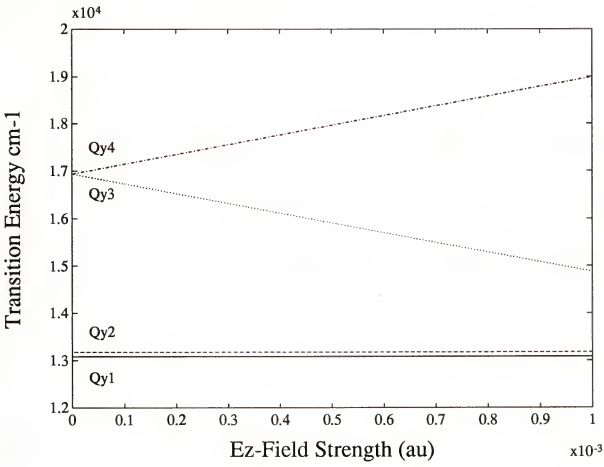

Figure 4.12 Effect of an electric field on the energy of the four Qy states of DMGBC at 5.0 Å separation. Field strength is given in atomic units (1 au. = 5.1419 x 10^{11} V/m) and transition energy is given in cm^{-1}. States are: Qy1 (—), Qy2 (- - -), Qy3 (.....), and Qy4 (-.-.-.-.).

The effect of the field on Qy3 and Qy4 makes their CT character evident while Qy1 and Qy2 remain largely unchanged. Qy1 retains all the calculated oscillator strength in these cases. Thus at large enough macrocycle separation, the contribution of the higher energy CR states (Qy3 and Qy4) to the low energy bands EX bands (Qy1 and Qy2) is minimal. As well, there is only a small red shift in the low energy Qy band of the dimer relative to the monomer.

The macrocycle separation was next reduced to 3.5 Å in the absence of any field. This separation corresponds closely to the bacteriochlorophyll dimers observed in *Rps. viridis* and *R. sphaeroides*. Table 4.18 summarizes the CI results for the Qy states in this case.

Table 4.18 DMGBC 3.5 Å Separation. Qy States CI Coefficients.

Qy-State	Qy1	Qy2	Qy3	Qy4
energy cm-1	12357.4	13421.5	14952.5	15472.5
osc. strength	1.1906	0	0	0.1043
Excitation	Exciton	Exciton	CR[1]	CR
d4 -> d5	-0.8850	0	0	-0.4114
d3 -> d6	0.3607	0	0	-0.9019
d4 -> d6	0	0.6989	-0.6706	0
d3 -> d5	0	-0.6213	-0.7415	0
d2 -> d7	0.2218	0	0	-0.0983
d1 -> d8	-0.1934	0	0	0.0878
d2 -> d8	0	0.2589	0.0163	0
d1 -> d7	0	-0.2419	-0.0157	0

1. Charge resonance.

States Qy1 and Qy2 have been shifted –724.3 cm^{-1} and +247.0 cm^{-1} respectively and states Qy3 and Qy4 by –1983.8 cm^{-1} and –1464.0 cm^{-1}, respectively, relative to the 5.0 Å case. Note, that not only is there a sizeable red shift of the lowest energy Qy band, but the two CR states exhibit a larger red shift that brings them energetically closer to states Qy1 and Qy2. This red shift of Qy3 and Qy4 is due to the enhanced overlap of the monomer wavefunctions which stabilizes these states. States Qy3 and Qy4 no longer exhibit a near degeneracy but are now split by 520 cm^{-1}. As well, the splitting between Qy1 and Qy2 has also increased. While Qy2 and Qy3 are still symmetry forbidden, Qy4 has gained oscillator strength while Qy1 has decreased in intensity. As the monomers are brought closer together the splitting of the dimer MOs (ie., d3–d4 splitting Figure 4.9) has increased. This decreases the dimer HOMO-LUMO gap. The net result of this is that the

symmetry allowed y-polarized configurations no longer occur in near degenerate pairs, while the symmetry forbidden y-polarized configurations still form near degenerate pairs. Thus the near degeneracy of the d4–>d5 and d3–>d6 symmetry allowed configurations is lifted. This is reflected in the unequal contributions of these two configurations to Qy1 and Qy4 (Table 4.18). It is also this unequal mixing that allows Qy4 to gain oscillator strength from Qy1 as the monomers are brought closer together. The symmetry forbidden y-polarized configurations (ie., d3–>d5, d4–>d6) still retain a near degeneracy which is reflected in the CI coefficients of Table 4.18. Physically, the increased oscillator strength of Qy4 makes sense, as excitations largely composed of CT character are stabilized by bringing the monomers closer together, and that oscillator strength increases as the monomer wavefunctions overlap more. In the SCF we observe that the dimer MOs have retained their LCMO description similar to the unperturbed 5.0 Å case with very small perturbations at atoms where the macrocycles overlap. In Table 4.19 we re-express the results of the CI in terms of this LCMO description.

Table 4.19 DMGBC 3.5 Å Separation. LCMO of Qy States.

Qy-State	Qy1	Qy2	Qy3	Qy4
energy cm-1	12375.4	13421.5	14952.5	15472.5
osc. strength	1.1906	0	0	0.1043
Excitation	Exciton	Exciton	CR[1]	CR
a2 -> a3	-0.6229	-0.6601	-0.0355	0.2452
b2 -> b3	0.6229	-0.6601	-0.0355	-0.2452
a2 -> b3	0.2622	-0.0388	0.7061	0.6566
b2 -> a3	-0.2622	-0.0388	0.7061	-0.6566
a1 -> a4	-0.2076	-0.2504	-0.0160	0.0931
b1 -> b4	0.2076	-0.2504	-0.0160	-0.0931
a1 -> b4	0.0142	-0.0085	-0.0003	-0.0053
b1 -> a4	-0.0142	-0.0085	-0.0003	0.0053

1. Charge resonance.

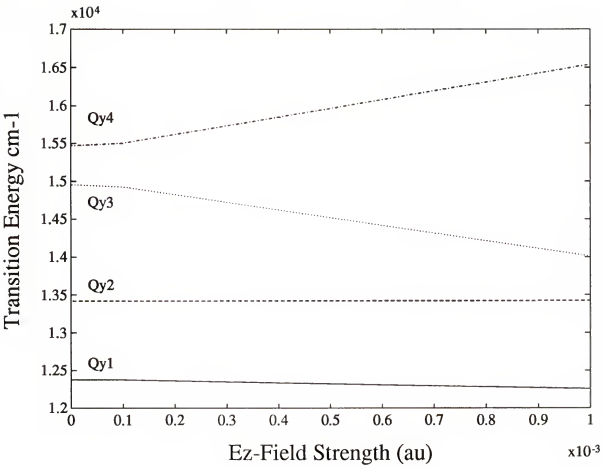

Figure 4.13 Effect of an electric field on the energy of the four Qy states of DMGBC at 3.5 Å separation. Field strength is given in atomic units (1 au. = 5.1419 x 10^{11} V/m) and transition energy is given in cm^{-1}. States are: Qy1 (—), Qy2 (- - -), Qy3 (.....), and Qy4 (-.-.-.-.).

The interaction of Qy1 and Qy4 is seen in the contribution of the EX a2–>a3 and b2–>b3 configurations to Qy4 and the contribution of the CT a2–>b3 and b2–>a3 configurations to Qy1. While Qy1 remains largely EX it has gained CR character from Qy4 and the latter has gained EX character and oscillator strength from Qy1. Due to the near degeneracy of the symmetry forbidden configurations, the magnitude of the interaction between Qy2 and Qy3 is much smaller, and they remain relatively unchanged when compared to the 5.0 Å case (Table 4.12).

We placed an E_z field of varying strengths across the dimer in an analogous fashion to the 5.0 Å case. Table 4.13 shows the effect of this on the Qy states transition energies. States Qy3 and Qy4 are sensitive to the presence of the E_z field while Qy1 and Qy2 remain largely unaffected by field strengths up to 10^{-3} au. Comparing Figures 4.12 and 4.13 it is evident that the shift in energy of states Qy3 and Qy4 is roughly half as great for the 3.5 Å separation case as it is for the 5.0 Å separation. We attribute this to the observation that for an equal amount of charge separation, the 5.0 Å case will produce a larger dipole moment than the 3.5 Å case. The energy of interaction of this dipole with the E_z field is greater for the 5.0 Å case than the 3.5 Å case. The calculated state dipole moments for 5.0 Å and 3.5 Å separations in the presence of a 10^{-6} au. E_z field are compared in Tables 4.17 and 4.20 respectively.

Table 4.20 DMGBC 3.5 Å Separation. State Dipole Moments[1] of Qy States With 10^{-6} au. E_z Field.

	μ_x	μ_y	μ_z
Ψ_o	0	0.0001	0.0003
Qy1	0	0.0041	0.0029
Qy2	0	0.0002	0.0004
Qy3	0	0.1158	0.0726
Qy4	0	-0.1198	-0.0745

1. Units are debyes.

Note the large difference in dipole moments for Qy3 and Qy4 for these two geometries. In Table 4.21 we show the LCMO description of the CI for the Qy states for 3.5 Å separation when the E_z field strength is increased to 10^{-4} au.

The CT contribution to states Qy3 and Qy4 favor b2–>a3 and a2–>b3 respectively. Note also that while Qy4 shares EX character with Qy1 (as in Table 4.19) Qy3 also has gained some EX character mainly a2–>a3 and consequently shows a small but finite calculated oscillator strength. State Qy2 remains largely unchanged relative the case with no field.

Table 4.21 DMGBC 3.5 Å Separation. LCMO of Qy States With 10^{-4} au. $\boldsymbol{E}_z$ Field.

Qy-State	Qy1	Qy2	Qy3	Qy4
energy cm-1	12374.4	13421.6	14924.0	15502.0
osc. strength	1.1896	0	0.0087	0.0966
a2 -> a3	-0.6234	0.6577	0.1026	-0.2310
b2 -> b3	0.6217	0.6625	-0.0322	0.2423
a2 -> b3	0.2487	0.0372	-0.5446	-0.8000
b2 -> a3	-0.2767	0.0407	-0.8307	0.4813
a1 -> a4	0.2078	-0.2496	-0.0409	0.0872
b1 -> b4	-0.0006	-0.2645	-0.0164	-0.0043
a1 -> b4	-0.0143	-0.0084	0.0012	-0.0052
b1 -> a4	0.0141	-0.0086	-0.0017	0.0050

Note that as the field strength is increased from 0 to 10^{-3} au. that Qy1 red shifts slightly (Figure 4.13) and decreases in intensity due to the increased CT character obtained from the interaction of Qy1, Qy3, and Qy4. Comparing with the 5.0 Å case we observe that as the macrocycles are brought closer together, CT configurations will contribute to the lowest excited state Qy1. For a symmetrical dimer this contribution remains CR in nature, while the application of an $\boldsymbol{E}$ field breaks this symmetry and induces net CT character not only to states Qy3 and Qy4 but to Qy1 as well. Typical Stark experiments employ field strengths as large as 10^8 V/m (about 10^{-4} au.). A large Stark effect has been observed in the lowest excited state of reaction centers of *Rps. viridis* and *R. sphaeroides* and has been attributed to an unbalanced CT occurring between the BChls of the special pair [86, 88, 31]. Due to an inherent asymmetry in the BChl special pair in reaction centers, from both structural and protein effects, the CT configurations contributing to the lowest excited state would be unbalanced and thus exhibit a net dipole moment difference and a greater response to an applied electric field than our model dimer.

Configurational Rotations

With the inter-macrocycle separation at 3.5 Å, monomer-A and monomer-B were

rotated by 15° and -15° respectively about the z-axis passing through the overlapping unsaturated rings (Figure 4.14). This configuration is suggested by the BChlb dimer of *Rps. viridis*. This arrangement removes the center of inversion but retains the C2 axis and allows mixing of the x and y-polarized configurations. Table 4.22 gives the result of the CI for the Qy states.

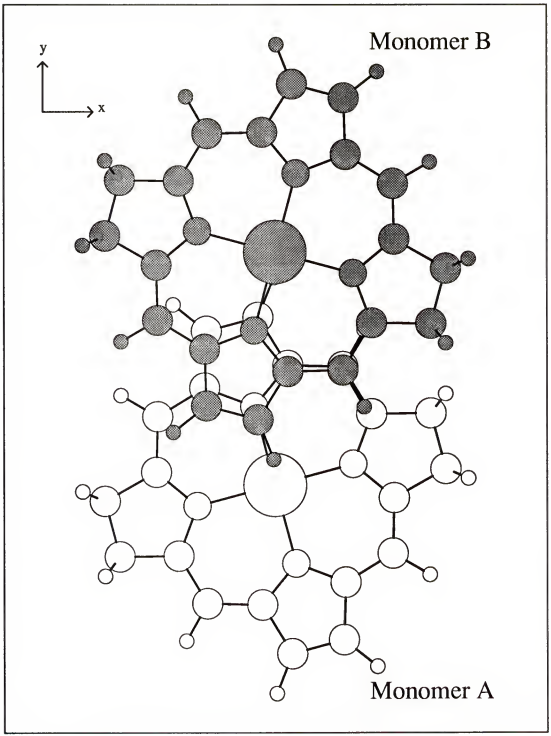

Figure 4.14 Configuration of the Mg-bacteriochlorin dimer at 3.5 ˝Å separation with monomer-A and monomer-B rotated by 15° and -15° respectively about the z-axis passing through their overlapping rings.

Table 4.22 DMGBC 3.5 Å Separation With Each Monomer Rotated 15° about Z–Axis. Qy States CI Coefficients.

Qy-State	Qy1	Qy2	Qy3	Qy4
energy cm-1	12302.6	13391.9	14724.0	15243.6
osc. strength	1.0993	0.0661	0.0037	0.1108
d4 -> d5	0.8894	0	0	-0.3740
d3 -> d6	0.3271	0	0	0.8970
d4 -> d6	0	0.7113	0.6430	0
d3 -> d5	0	0.5911	-0.7518	0
d2 -> d7	-0.2100	0	0	-0.0978
d1 -> d8	0.1908	0	0	0.0945
d2 -> d8	0	-0.2538	0.0236	0
d1 -> d7	0	0.2373	-0.0243	0
d4 -> d7	0.0003	0	0	-0.0924
d3 -> d8	0.0422	0	0	-0.0500
d4 -> d8	0	-0.0251	0.0553	0
d3 -> d7	0	0.0151	0.0378	0
d2 -> d5	-0.0132	0	0	-0.0831
d1 -> d6	-0.0111	0	0	0.0573
d2 -> d6	0	0.0180	0.0198	0
d1 -> d5	0	-0.0033	-0.0138	0

There is a small but finite contribution from the x-polarized transitions to the Qy states. Correspondingly there is a similar contribution to the Qx states from the y-polarized transitions (data not shown). Note that transitions d4–>d8, d3–>d7, d2–>d6, and d1–>d5 are strongly allowed x-polarized transitions. Consequently states Qy2 and Qy3 have gained finite oscillator strength and their transition moments are x-polarized. Similarly, states Qx2 and Qx3 have contributions from strongly allowed y-polarized transitions and have a small but finite oscillator strength and y-polarized transition moments (data not shown). State Qy1 has oscillator strengths in the nonrotated and rotated case, of 1.1906 and 1.0993 respectively. The decrease in calculated intensity is due primarily to

the mixing with the Qx states. The Qy and Qx states are respectively slightly red and blue shifted from the nonrotated 3.5 Å case (Table 4.18) again indicating a configuration mixing and splitting between the x and y-polarized states as the macrocycles are rotated.

We next compared the electric field response of the 3.5 Å separation rotated and nonrotated cases. Table 4.23 lists the calculated transition energies of the Qy states for the two cases with 10^{-3} a.u. E_z and E_y fields.

Table 4.23 DMGBC 3.5 Å Separation With Zero Field, 10^{-3} au. E_z and E_y Fields. Qy States Transition Energies for Rotated and Nonrotated Configurations.

	Non-Rotated Transition Energy cm-1 (Field Polarization)			Rotated Transition Energy cm-1 (Field Polarization)		
Transition	No Field	Ez	Ey	No Field	Ez	Ey
Qy1	12375.4	12256.5	12082.6	12302.6	12167.7	11996.8
Qy2	13421.5	13422.8	13441.9	13391.9	13396.2	13391.3
Qy3	14952.5	14011.2	13639.7	14724.0	13866.3	13591.8
Qy4	15472.5	16540.2	17299.3	15243.6	16227.9	16841.5

For both the rotated and nonrotated configurations the calculated shifts in the Qy bands are greater for the E_y field relative to the E_z field. Since the Qy states are y-polarized, a greater field response to an E_y field is expected. The splittings between Qy3 and Qy4 for both the E_y and E_z fields are larger in the nonrotated vs. the rotated configuration. In the presence of the E_y field Qy3 red shifts 180.6 cm^{-1} and Qy4 blue shifts 228.9 cm^{-1} more for the nonrotated vs. the rotated case. The rotation of the macrocycles reduces the distance between charges localized on the respective macrocycles. Since the field response should be proportional to the induced dipole for these CR states, we would expect smaller shifts for CR states in the rotated case.

Discussion

Extension of the 4–orbital model to an 8–orbital model in dimers of MGBC results in four Qy states that make up the low energy spectrum of DMGBC. In our model system we transform the results of the CI of DMGBC to a basis of monomer excited configurations and show that two excitonic (EX) and two charge resonance (CR) states arise as a natural consequence of this treatment. In this sense the coupled-chromophore model can be viewed as a subset of MO theory [81, 82]. When the monomer units of DMGBC are separated by 5.0 Å, the lowest energy Qy1 state is calculated to carry all of the Qy band oscillator strength and is composed almost entirely of EX contributions in the LCMO (monomer basis) description. States Qy2, Qy3, and Qy4 all have zero calculated oscillator strength and are characterized as EX, CR, and CR respectively. Thus, not surprisingly, at large separation the CT configurations show no appreciable contributions to the low lying EX states, even in the presence of an electric field perturbation. As the macrocycles are brought closer together, the symmetry allowed CR state, Qy4, gains oscillator strength from Qy1. This is due to the increased splitting of the dimer MOs which removes the near degeneracy of the symmetry allowed configurations that contributed to states Qy1 and Qy4. In an LCMO interpretation this is also due to the increased overlapping of the monomer wavefunctions involved in the CR cross excitations. The application of an electric field removes the C2 axis and center of inversion allowing the four Qy states to mix. This mixing removes the balance in the CR states, Qy3 and Qy4, giving each state net charge transfer (CT) character in the presence of the field. Thus we calculate field induced splittings of the CR states that are dependent on the magnitude of the applied field (figs. 4, 5). These field induced splittings of the CR states Qy3 and Qy4 are greater at 5.0 Å separation than 3.5 Å separation due to the larger interaction of the resulting charge separation with the field. At 3.5 Å separation this splitting of the Qy3 and Qy4 states and their mixing, not only with each other but also with Qy1, causes Qy3 to also gain EX character and oscillator strength. Correspondingly, Qy1 is predicted to lose

oscillator strength due to its increased CT character. The Qy1 transition energy red shifts slightly and loses intensity at higher field strengths due to this CT contribution (Figure 4.13). Tables 4.24 and 4.25 illustrate the different interactions of the four Qy states with increasing field strength for 5.0 Å and 3.5 Å separation respectively, in nonrotated configurations. At 5.0 Å separation the presence of the E_z field causes Qy3 and Qy4 to mix (Table 4.14) which results in Qy3 and Qy4 being dominated by strong CT states, b2–>a3 and a2–>b3 respectively (Table 4.16). In the presence of a 10^{-6} au. E_z field, this results in 0.9986 B->A and 0.9986 A->B net electrons transferred for Qy3 and Qy4, respectively (Table 4.24).

Table 4.24 DMGBC 5 Å Separation. Net Charge[1,2] Separation for Qy States with E_z Field.

	Qy1		Qy2		Qy3		Qy4	
E_z Field (au.)	Net CT	Osc. Str	Net CT.	Osc. Str.	Net CT.	Osc. Str.	Net CT.	Osc. Str.
0.0	0.0000	1.2628	0.0000	0.0000	0.0000	0.0000	0.0000	0.0000
-10^6	0.0000	1.2628	0.0000	0.0000	0.9986	0.0000	-0.9986	0.0000
-10^3	0.0001	1.2629	0.0000	0.0000	0.9999	0.0000	-1.0000	0.0000

1. Units are electrons.
2. Positive (negative) indicates net charge transferred from B->A (A->B).

At 5.0 Å separation, there is relatively little interaction of Qy3 and Qy4 with Qy1 and Qy2. The latter two remain almost entirely EX character and Qy1 retains all the calculated oscillator strength. These calculations predict the CT state Qy3 to cross the Qy1 band at field strengths of about 0.002 au.

The interactions are quite different in the 3.5 Å case. We observe that at zero field strength Qy4 has oscillator strength gained from Qy1. Qy1 now contains balanced CR contributions from Qy4 and the latter has EX contributions from Qy1 (Table 4.19). As the E_z field strength is increased there is substantial interaction of states Qy1, Qy3, and Qy4.

As Qy3 and Qy4 split in energy, Qy3 begins to interact with Qy1 and gains intensity from both Qy1 and Qy4 . We see increasing EX character in Qy3 which accounts for its increased calculated oscillator strength. State Qy1 gains CT character from Qy3, loses intensity, and red shifts slightly. At a field strength of 10^{-3} au. Qy1 shows a 0.2046 B->A net electrons transferred while Qy3 now exhibits 0.7256 B->A net electrons transferred (Table 4.25).

Table 4.25 DMGBC 3.5 Å Separation. Net Charge Separation[1,2] for Qy States with E_z Field.

	Qy1		Qy2		Qy3		Qy4	
E_z Field (au.)	Net CT	Osc Str.	Net CT.	Osc. Str.	Net CT.	Osc. Str.	Net CT.	Osc. Str.
0.0	0.0000	1.1906	0.0000	0.0000	0.0000	0.0000	0.0000	0.1043
-10^6	0.0002	1.1906	0.0000	0.0000	0.0043	0.0000	-0.0045	0.1043
-10^3	0.2046	1.0622	0.0067	0.0037	0.7256	0.2026	-0.9372	0.0278

1. Units are electrons.
2. Positive (negative) indicates net charge transferred from B->A (A->B).

This is in marked contrast to the equivalent case for 5.0 Å separation where Qy1 exhibits essentially no net CT (Table 4.24). For this 3.5 Å case state Qy4 shows 0.9372 A->B electrons transferred which is nearly the same as the sum of Qy1, Qy2, and Qy3. Note that not only do the oscillator strengths of the four Qy states show a relatively constant sum but, for any given field strength, the net CT from B->A is nearly equal to the net CT from A->B. Thus we observe that when the macrocycles are brought into close juxtaposition for this particular geometry there exists a mechanism for generating a low energy reasonably intense transition that exhibits charge separation, albeit at high field strengths. For this model system we have used $\boldsymbol{E}$ fields to induce perturbations to an otherwise symmetric dimer and thus, we are essentially calculating the interaction of induced dipole differences with the $\boldsymbol{E}$ field. The BChlb dimer *in vivo* exhibits not only conformational asymmetry, but is further affected by nearby protein moieties. The

presence of nearby partially charged groups could generate large local nonhomogeneous fields that are known to have substantial effects on the calculated optical properties of chlorophyll systems [37, 36, 49]. Thus, dimers of BChlb can exhibit nonzero calculated dipole moment differences between the ground and excited states in the absence of any applied external fields. Hence electrochromic effects on these systems will be more pronounced than on the DMGBC model in this study.

When the macrocycles were rotated 15° at 3.5 Å separation, in a configuration that retained an overlap of the unsaturated rings (Figure 4.14) we calculated a small mixing of the x and y-polarized configurations. This mixing allows the formerly symmetry forbidden Qy2 and Qy3 (Qx2, and Qx3) states to gain oscillator strength from the strongly allowed x-polarized (y-polarized) transitions. If this mixing were additionally affected by closer macrocycle distances, the presence of charged or polar residues, the presence of ring V and symmetry breaking polar side groups, or geometric asymmetries between the monomers, we would expect to observe a broadening in the low energy transitions. Not surprisingly, the field response of the Qy states was greater for E_y than E_z fields.

Our present examination of a simple dimer model provides the starting point for an extension to the electronic properties of the excited state surfaces of the more complicated BChlb dimer in *Rps. viridis*. While the actual BChlb dimer does not behave strictly as a coupled chromophore, we are able to demonstrate the presence of four low lying electronic excited states in INDO/S calculations of the special pair of *Rps. viridis* that exhibit Qy origin similar to our study here. At monomer distances much less that 3.5 Å we observe that the MGBC dimer begins to behave as a supermolecule (data not shown) and the quality of a coupled-chromophore model decreases. In addition, the red shift can become quite large when the chromophores have contacts less than about 3.0 Å [67]. The most recent X-ray coordinates for the reaction center of *Rps. viridis* show that the average spacing in the BChlb special pair is about 3.3 Å [9, 8, 10].

The special pair appears to be a fundamental structure in most photosynthetic systems.

In these cases, energy transfer is effective between antennas, and reaction centers on a picosecond timescale. For this efficiency, the lowest energy band of the reaction center must lie lower in energy than the corresponding lowest lying excited states of the antenna. Although electrochromic effects[37, 36, 49], and geometric variations of the macrocycle may contribute to this property, formation of the dimer would be a simple and robust way to ensure that the reaction center possessed the Qy band of lowest energy [67]. Furthermore, the delocalization of charge in a hydrophobic environment would be more favorable in a dimer, while intermacrocycle geometry changes could enhance not only the forward electron transfer rate but inhibit back reactions.

CHAPTER 5
THE BACTERIOCHLOROPHYLL–B DIMER FROM *Rhodopseudomonas viridis*

Introduction

The BChlb dimer in the photosynthetic RC of *Rps. viridis* has the UV/vis excitation of lowest energy[12]. This band in the BChlb dimer can be excited either directly or by energy transfer from the surrounding BChlb containing antenna proteins whereupon a very rapid initial electron transfer event takes place from the BChlb dimer to a bacteriopheophytin–b (BPhb) along one of the chromophore branches (Figure 1.3). The BChlb dimer is known as the primary electron donor (P). The mechanistic details of this initial electron transfer reaction are not well understood. Indeed there is still debate as to the role of the auxiliary BChlb in the initial electron transfer event perhaps even being the primary electron acceptor. However, the pivotal role of P as the primary electron donor has made it the subject of much investigation. A great deal of experimental and theoretical work has been done in attempts to elucidate the nature of the excited states of P and how its photophysical properties are affected by its protein environment [13, 12] (and references within).

The structure of the BChlb dimer is shown in Figure 5.15. The BChlb monomers are labelled as to their major association with either protein subunits L or M. The macrocycles are cofacial with rings I overlapping and are rotated with respect to one another about an axis that is roughly perpendicular to the macrocycles planes. The Mg atoms are out of the plane of the macrocycles and have their exterior fifth ligand positions occupied by histidine sidechains from the proteins (not shown). Unlike the model dimers studied in Chapter 4, the BChlb dimer from the RC of *Rps. viridis* does not exhibit strict structural

C2 symmetry. Also, the macrocycle planes are not strictly planar, with $BChlb_M$ being slightly more puckered relative to $BChlb_L$. Furthermore there are asymmetric interactions of the BChlb dimer with nearby amino acid sidechains from the protein.

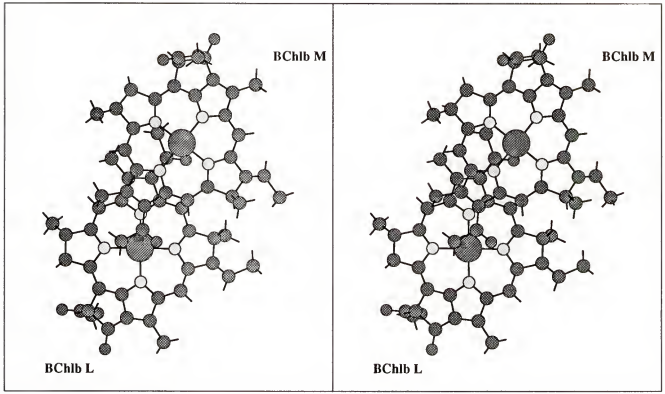

Figure 5.15 Stereo view of the bacteriochlorophyll-b dimer from *Rps. viridis*. The phytol chains from connected to ring IV have been truncated. The macrocycles are labelled as to their major association with protein subunits L or M.

The experimental spectroscopic properties of P reflect the lack of strict C2 symmetry in the RC. The lowest excited state of the RC (known as the $P_{(-)}$ band) exhibits a large Stark effect. These Stark experiments show the change in state dipole moment for $P_{(-)}$ to be roughly 8 Debye relative to the ground state[83]. This large charge redistribution in $P_{(-)}$ is characteristic to all bacterial RCs studied to date. How or why it occurs is still unknown. Also, linear dichroism (LD) studies [92] of the RC indicate that the two lowest lying excited states (both attributed to P) are polarized roughly perpendicular and parallel to the pseudo C2 axis that extends from the nonheme Fe(II) atom to P (Figure 1.3).

The lowest excited state of P is not the electron transfer band. However, the charge separated state resulting from the primary electron transfer event must surely evolve dynamically from the excited state surface of $P_{(-)}$. In this chapter we will describe the results of theoretical studies aimed at understanding the electronic structure of the low lying excited states of P. We attempt to answer several questions:

- How is charge density redistributed in the lowest excited state of P
- What specific structural and environmental parameters dictate the nature of this charge redistribution
- Can 'dissecting' the low lying excited states in a similar fashion to Chapter 4 help us understand the anomalous red shift and charge redistribution of $P_{(-)}$

Results and Discussion

The electronic structure calculations of the ground state and excited states utilized the semi-empirical INDO/S method[38–40]. The coordinates of the heavy atoms of the structures studied were obtained from the X-ray data of Deisenhofer refined to 2.3 Å resolution[7–9]. The hydrogens were attached by standard rules and checked to ensure that no unacceptable steric interactions were generated. Except where stated explicitly, the heavy atom coordinates utilized were not altered or optimized further from the X-ray data. The phytol side chains on each BChl were truncated (Figure 5.15).

Figure 5.16 shows the INDO/S spectrum calculated for the BChlb dimer for energies up to 25000 cm^{-1}. This calculation does not include any of the nearby amino acids. The excited states have been assigned labels Qy1–Qy4, and Qx1–Qx4. The meaning of these labels was developed in Chapter 4. The two lowest energy transitions, labelled Qy1 and Qy2, correspond to the experimentally observed transitions of the RC $P_{(-)}$ and $P_{(+)}$ respectively. The experimental labels designate them as the lower and upper exciton components of the BChlb dimer. The labels given in Figure 5.16 will be used for the remainder of this chapter. Qy1 occurs at an energy of 10786 cm^{-1}. This represents

an 1850 cm^{-1} red shift relative to the average of the Qy transitions of the respective monomers (Chapter 3).

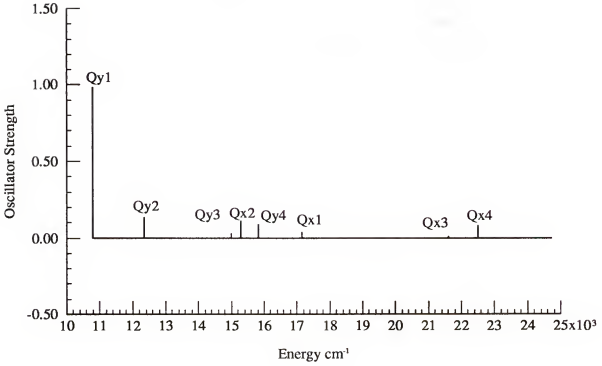

Figure 5.16 INDO/S calculated UV/vis spectrum for BChlb dimer up to 25000 cm^{-1}. The calculations included 785 configurations in the CI.

To label the excited states in Figure 5.16 we performed an LCMO analysis similar to that outlined in Chapter 4. However, unlike the model dimer study, the real BChlb dimer lacks rigorous C2 symmetry. Thus we will observe a mixing of the x– and y–polarized states. Also, due to the lack of an inversion center, there will be no symmetry forbidden transitions as in the model dimer. Furthermore, the BChlb dimer has a non–zero dipole moment and the electronic wavefunctions of the BChlb monomers overlap and interact more strongly than the model dimer cases studied. Thus, the coupled chromophore model

is not strictly applicable to the BChlb dimer for obtaining a quantitative description of the electronic excited states. Given all this, we still can apply the LCMO analysis to obtain a qualitative sense of the 'monomer origins' of the excited states of the BChlb dimer. We do this in hope of being able to study the specific perturbations that the nearby protein environment incurs upon the BChlb dimer, albeit in a qualitative sense.

We expanded the BChlb dimer MOs in a basis of the relevant monomer MOs.

$$\psi_i^{dimer} = \sum_{A}^{monomers} \sum_{\mu \in A}^{MOs} |\phi_\mu\rangle\langle\phi_\mu|\psi_i^{dimer}\rangle \qquad (5.2.1)$$

If we examine the four HOMOs and four LUMOs of the BChlb dimer we observe that they are decomposed almost entirely (> 95%) of the two HOMOs and two LUMOs from each BChlb monomer. These eight dimer MOs constitute the 8–orbital manifold we will use to examine the low lying excited states of the dimer and shown in Figure 4.9. Using these decomposed dimer MOs we can re-express the results of the CI of the dimer in terms of the basis of monomer excitations. Table 5.26 shows the LCMO decomposition of the four Qy states of the BChlb dimer. We show only the contributions of the monomer excitations that derive from the y-polarized configurations (Figure 4.9 and Table 4.12) and contribute the most to the Qy states. Similar analysis was used to label the Qx states (not shown).

Table 5.26 BChlb dimer Qy states expressed as LCMOs.

Qy State	Qy1	Qy2	Qy3	Qy4
energy cm^{-1}	10786.4	12345.1	14995.5	15820.4
oscillator str.	0.9835	0.1357	0.0305	0.0881
a2 -> a3	0.6503	-0.5618	-0.2714	0.2696
b2 -> b3	0.5588	0.6590	0.2672	0.3287
a2 -> b3	0.3448	-0.2447	0.6684	-0.5802
b2 -> a3	0.3015	0.3296	-0.6053	-0.6589
a1 -> a4	0.1925	-0.2066	-0.0969	0.0900
b1 -> b4	0.1198	0.1880	0.0645	0.0906
a1 -> b4	0.0142	0.0185	0.0097	0.0085
b1 -> a4	0.0142	-0.0152	-0.0075	0.0092

This initial configuration of the BChlb dimer roughly corresponds to a configurationally perturbed DMGBC 3.5 Å model dimer (Figure 4.14). Note that Qy1 and Qy2 are composed mainly of excitonic local excitations (EX) (a2–>a3 and b2–>b3) while Qy3 and Qy4 are dominated by charge transfer (CT) cross excitations (a2–>b3 and b2–>a3). Thus the experimental assignment of $P_{(-)}$ and $P_{(+)}$ to the lower and upper exciton components of the dimer is qualitatively in agreement with our results. In a symmetrical model dimer, Qy1 and Qy2 correspond to pure EX states while Qy3 and Qy4 would correspond to balanced CT states, or charge-resonance (CR) states. Note the contribution of CT transitions to Qy1 and Qy2. We observe that the CT transitions a2–>b3 and b2–>a3 are unbalanced in both Qy1 and Qy2. In fact Qy1 exhibits slight $BChlb_L$ –> $BChlb_M$ shift of charge density based on this analysis. A simple coupled chromophore analysis composed on only local excitations would not be able to describe this CT contribution to the Qy states and would be unable to predict a large red shift in the Qy1 band (Chapter3). The possibility of inter-macrocycle CT contributions to the low lying excited states of the BChlb dimer was postulated and modelled by Warshel and Parson[77, 78]. In their coupled chromophore model, they included explicit CT transitions and varied

their energies until their calculated spectrum agreed with absorption, LD, and circular dichroism (CD) results. Indeed their model showed that CT transitions could contribute to the red-shift of Qy1. However a somewhat arbitrary relative placement of $BChlb_L$ –> $BChlb_M$ and $BChlb_M$ –> $BChlb_L$ CT states was required for their analysis[77, 78]. We demonstrate here that the internal CT states are a natural consequence of the calculation on the supermolecule and we can qualitatively project out their contribution to the low lying excited states from our calculation. Unlike Parson and Warshel, we predict a slight $BChlb_L$ –> $BChlb_M$ net CT in Qy1. However we find that the direction and amount of net CT in Qy1 is sensitive to geometry. We observe that Qy3 and Qy4 have finite calculated oscillator strength. We attributed this to the contributions of EX transitions in these states as shown in our LCMO results Table 5.26. Experimentally we would not expect to observe Qy3 and Qy4 directly. They would have low oscillator strength and be "buried" within the broad absorptions of the Qy bands of the other chromophores of the RC. Small changes in geometry of the BChlb dimer could modulate the mixing of these four Qy states and alter the net CT character in Qy1 from Qy3 and Qy4. There is an enhanced mixing of the x- and y-polarized configurations in the BChlb dimer relative to the model dimer. Thus we observe that Qy2 has acquired x-polarized contributions as it did in the DMGBC model dimer study of Chapter 4. This has a consequence in the calculated LD of Qy2 giving it a component perpendicular to Qy1.

The BChlb dimer has specific interactions with several amino acids in the protein[93]. The asymmetry of CT in the RC along the L-branch and the possibility of internal CT character in the excited states of the BChlb dimer have been attributed in part to these amino acids. Indeed the hydrogen bonding of a glutamic acid residue (L104) to the bacteriopheophytin on the L-branch in RCs of *Rhodobacter capsulatus* is known to have a large enough effect on the UV/vis absorption of that chromophore that it can be distinguished from its M-branch counterpart[94]. We list in Table 5.27 the two amino acid residues that ligate to the Mg atoms of the BChlb dimer and the three that hydrogen

bond to the macrocycle ring substituents for *Rps. viridis*. There are hydrogen bonding

Table 5.27 Amino Acid Residues that Interact with BChlb dimer

Amino Acid	Interaction
Histidine L173	$BChlb_L$ Mg ligand
Histidine M200	$BChlb_M$ Mg ligand
Threonine L248	H-bonded to ring V keto of $BChlb_L$
Histidine L168	H-bonded to ring I acetyl of $BChlb_L$
Tyrosine M195	H-bonded to ring I acetyl of $BChlb_M$

interactions with ring I acetyl groups for both BChlb monomers. In addition, there is a hydrogen bonding amino acid (Thr L248) that interacts with the ring V keto of $BChlb_L$. We have shown in Chapter 2 that charged points near ring I or ring III/V side if BChlb macrocycles can have substantial effects on the calculated properties. Thus the possibility exists for these hydrogen bonding amino acids to exert effects on the BChlb dimer's photophysical properties and possibly enhance the asymmetry of its excited states.

We show in Table 5.28 the calculated UV/vis transition energies and oscillator strengths of Qy1 and Qy2 for the BChlb dimer in the presence of the amino acids listed in Table 5.27. The H–bonding hydrogens have been given bond lengths of about 0.9–1.0 Å with their respective amino acid side chains based on X-ray crystallographic results [Fajer, J., personal communication]. We find that the ligating amino acids (L173

Table 5.28 Effects of amino acids on the Qy1 and Qy2 states of the BChlb dimer

Structure	Qy1		Qy2		Qy1-Qy2 Splitting
	Energy cm^{-1}	Oscill. Str.	Energy cm^{-1}	Oscill. Str.	cm^{-1}
Experiment (295K)	10400	-	11765 [d]	-	1365 [d]
BChlb Dimer	10786	0.9835	12345	0.1357	1559
Dimer + L173, M200	10982	0.9482	12490	0.1311	1509
Dimer + L248, L168, M195	10585	1.0089	12230	0.1378	1645
Dimer + all amino acids [a]	10756	0.9735	12335	0.1311	1579
Dimer + all amino acids (+0.1 Å H-bonding) [b]	10679	0.9729	12254	0.1336	1575
Dimer + all amino acids (L168 modified H-bonding) [c]	10459	0.9987	12108	0.1274	1649

a: BChlb dimer plus amino acids L173, M200, L248, L168, M195 (Table 5.27).

b: The H-bonding hydrogen for L248, L168, and M195 have all had their bond lengths increased by 0.1 Å.

c: The H-bonding hydrogen for L168 has had its bond length increased by 0.35 Å.

d: This value is subject to some degree of uncertainty as there is an overlapping with the Qy bands of the remaining chromophores of the RC that increases with T.

and M200) alone contribute to a blue-shift relative to the "naked" BChlb dimer for Qy1 and Qy2 of about 200 cm^{-1} and 150 cm^{-1} respectively. The H-bonding amino acids (L248, L168, M195) with normal bond lengths for the H-bonding hydrogens cause a red-shift for Qy1 and Qy2 relative to the naked dimer of about 200 cm^{-1} and 115 cm^{-1} respectively. All of these amino acids present simultaneously give a very small net red-shift in both Qy1 and Qy2. An LCMO analysis of these structures shows the same overall qualitative results of Table 5.26 for the naked dimer (data not shown). The net asymmetry in the lowest CT transitions a2 –> b3 and b2 –> a3 is in fact reduced in the BChlb dimer with all five amino acids present. Plato et al. have found that when

these nearby amino acids are modelled as point charges placed at their atomic positions, they enhance the asymmetry in the HOMO for the BChlb dimer. They have used this argument to claim a $BChlb_L$ –> $BChlb_M$ net CT character in the lowest excited state of the BChlb dimer that enhances the overlap of MOs for the L-branch vs. the M-branch[84, 31]. Their calculations did not include a CI to calculate the actual excited states. Also they utilize a modified parameterization in their INDO method to reproduce calculated spin densities, and they optimized the geometry of parts of the BChlb dimer to produce a better agreement between calculated and experimental spin densities[68, 95]. By optimizing their method and the geometry of the BChlb dimer to agree with spin densities (from the BChlb cation radical and the BChlb triplet radical) their structure is somewhat different than ours. We have found that small geometric changes in the BChlb dimer can invoke large changes in some calculated properties. Also it is thought that in the photoionization process these geometry changes are important and they greatly separate the first excited state surface of closed shell BChlb dimer from the spin doublet or triplet species which are relatively long lived and have a chance to relax. Thus a direct comparison of our results with the results of Plato is difficult and perhaps inappropriate.

It is thought that small movements in the H-atoms of H-bonding groups can be quite rapid and exert large effects on CT reactions[96]. Therefore we modified the placement of the H-bonding hydrogens for L248, L168, and M195 by lengthing their H-amino acid bond lengths by 0.1 Å relative to the amino acid oxygen atom to which it is bonded (Table 5.28). The calculated energies of Qy1 and Qy2 are 10679 cm^{-1} and 12254 cm^{-1} respectively. Lengthening just the H-bonding hydrogen for L168 (H-bonded to ring I acetyl of $BChlb_L$) by 0.35 Å gives a Qy1 energy of 10459 cm^{-1}. This has caused a red shift of about 300 cm^{-1} relative to the normal amino acid H-bonding bond lengths (Table 5.28) and approaches the experimental value of 10400 cm^{-1}. Note that due to the overlapping of Qy2 with the Qy transitions of the other chromophores in the reaction center, the placement of Qy2 at room temperature is somewhat difficult. Lengthening the

H-bond tends to render the H-bonding hydrogen more positive and enhances the dipole of the amino acid–hydrogen group. This exerts an enhanced electrochromic effect in the vicinity of the BChlb dimer. We have seen in Chapter 2 that positive charges in the vicinity of ring I can cause large red shifts in the Qy transition energy. Thus we observe a 300 cm^{-1} red shift in Qy1 when we lengthen the H-bond for L168 by 0.35 Å. While we have probably created too strong an electrochromic effect we wish to merely demonstrate that small movements in the H-bonding hydrogens can have noticeable effects on the calculated UV/vis absorption of the BChlb dimer.

We define a pseudo C2 symmetry axis for the RC that consists of a line connecting the nonheme Fe(II) atom and the average coordinates of the two Mg atoms of the BChlb dimer. The angle of the transition moments of our calculated UV/vis spectra with this axis can be compared to results from linear dichroism (LD) data on intact reaction centers from *Rps. viridis*[92]. Table 5.29 gives these values for states Qy1 and Qy2 for the structures we have examined as well as experimental values from the reaction center. In

Table 5.29 Calculated LD angle for BChlb dimer structures compared with experiment

Structure	Qy1 LD angle (degrees)	Qy2 LD angle
Experiment [92]	90	30
naked BChlb Dimer	95	8
Dimer + L173, M200	85	12
Dimer + L248, L168, M195	85	4
Dimer + all amino acids[a]	95	6

a: BChlb dimer plus amino acids L173, M200, L248, L168, M195 (Table 5.27).

all cases we have fairly good agreement with experiment for Qy1. The LD angle for Qy2 appears to be more sensitive to the specific structure examined. This is due in part to the smaller calculated intensity of Qy2 since small changes in the transition moment vector represent a larger percentage of the calculated oscillator strength and could give

proportionately larger changes in the LD angle. In addition to our analysis of Qy2 in Table 5.26 our data here also strengthens the identification of the shoulder at 850 nm in the experimental spectrum (and labelled $P_{(+)}$) as being largely attributed to the BChlb dimer. This identification has been the subject of some controversy in the past[97].

Small geometric changes in the BChlb dimer can have effects on the calculated UV/vis spectrum. Low frequency inter-macrocycle modes that vibronically couple with the electronic transition have been thought to play a role in effecting the band width of the low energy absorbtion of intact reaction centers[98]. This band exhibits roughly a 1000 cm^{-1} band width at 295K that decreases to roughly 500 cm^{-1} at 5K[98]. As well, this band red shifts approximately 300 cm^{-1} over the same temperature range. The red shift has been attributed to contraction of the reaction center protein complex which is though to bring the BChlb monomers of the BChlb dimer closer together. This should increase their exciton splitting and red shift the low energy band. Early INDO/S calculations on the BChlb dimer from the 3.0 Å refined X-ray crystal structure had the macrocycles of the BChlb dimer about 0.3 Å closer together than seen in the later more highly refined crystal structure. The calculated energy for Qy1 in that study was 9339 cm^{-1}[67] a large red shift relative to the more recent calculations above (Table 5.28). Using the coordinates of the naked BChlb dimer in the present study, if we increase the average intermacrocycle separation by 0.2 Å we calculate Qy1 at 11393.1 cm^{-1} which represents a blue shift of 607 cm^{-1}. This merely demonstrates the sensitivity of the calculated Qy bands to macrocycle separation. The Qy1 band is also sensitive to rotation of the macrocycle's acetyl group on ring I. For $BChlb_M$, we rotated the ring I acetyl group by 25° out of the mean macrocycle plane. This movement did not produce any unfavorable steric constraints. The calculated transition energy of Qy1 is now 10916.9 cm^{-1} which is a blue shift of about 130 cm^{-1}.

We have demonstrated that calculations on the BChlb dimer can give reasonable agreement with experiment for several characteristics of the low energy UV/vis spectrum.

The presence of four Qy bands is demonstrated and their connection with simpler exciton based models discussed. The two lowest energy Qy bands that have appreciable oscillator strength are compared with the experimentally observed $P_{(-)}$ and $P_{(+)}$ from intact reaction centers. Good agreement is obtained between the calculated and observed transition energy and relative intensities of these bands. Furthermore our LD results are in good agreement with experiment which show that Qy1 is polarized largely perpendicular to the molecular C2 axis while Qy2 is more parallel with this C2 axis. The placement of the local y-axis of each BChlb monomer's macrocycle is roughly perpendicular to the C2 axis and thus the excitonic coupling of the local Qy transitions should give a transition roughly perpendicular to the C2 axis. We saw in our study of model dimers (Chapter 4) that Qy2 gained oscillator strength in the rotated case largely from the strongly allowed x-polarized transitions. This contribution to Qy2 here would explain the more parallel polarization of Qy2 with the C2 axis for the BChlb dimer. Our calculations strengthen the identity of the shoulder observed at 850 nm (and attributed to $P_{(+)}$) with a BChlb dimer band largely dominated by excitonic transitions. Furthermore we demonstrate the contribution of CT transitions to the Qy1 and Qy2 bands. The BChlb dimer is held within the protein scaffold by its interactions with the surrounding amino acids and other chromophores present. Our calculations that include several of the nearby amino acids, specifically those that ligate to the Mg atoms of the BChlb dimer and hydrogen bond to the macrocycles and their substituents, show small changes in the calculated properties of the BChlb dimer. However we show that small movements in the H-bonding hydrogens can elicit fairly large effects on the calculated UV/vis spectrum. These effects are seen to be largely electrochromic and can be understood in terms of the simple charge-dipole model developed in Chapter 2. Also we observe that small changes in geometry can have sizeable effects on the calculated UV/vis spectrum. Specifically, the contributions of low frequency modes in the BChlb monomers, such as rotating motion of the ring I acetyl, may play an important role in determining the band width and initiation of

photosynthetic charge transfer.

CHAPTER 6
THE PHOTOSYNTHETIC REACTION CENTER OF *Rhodopseudomonas viridis*

Introduction

To understand the photophysical properties of bacterial photosynthetic reaction centers (RC) and the process of light driven electron transfer we must address the properties of the chromophores as an aggregate as well as their interactions with the surrounding protein. The chromophores in the reaction center of the photosynthetic bacterium *Rps. viridis* are shown in Figure 6.17. There are four bacteriochlorophyll-b's (BChlb) two bacteriopheophytin-b's (BPhb) two quinones, and a nonheme iron atom. The phytol tails of the BChlbs and BPhbs have been truncated for clarity as have the chelating ligands to the Fe atom. The surrounding protein acts noncovalently as a scaffold to maintain the relative orientations of these chromophores. To study the RC theoretically is a large undertaking. The entire protein-pigment complex contains in excess of 10000 heavy atoms. Considering just the chromophores with hydrogens added there are roughly 1100 atoms. We would like to be able to calculate the electronic propterties of at least the chromophore aggregate of the RC. This system is too large to be effectively studied by current *ab initio* methods. While the phenomenological coupled chromophore type models are capable of handling a system of this size they often require extensive and arbitrary fitting to reproduce experimental data.

We chose to use the semi-empirical INDO/S method to study a model of the chromophore aggregate of the RC[38–40]. While semi-empirical methods do require some parameterization based upon experiment, there is no need to explicitly parameterize the

model on the specific system under study as is often the case for the coupled chromophore model. The INDO/S SCF-CI model has been directly parameterized on the singles excited configuration interaction (CI) level to reproduce the spectra of benzene and pyridine and the diazenes[38].

We will be particularly interested in the preference for the L branch over the M branch for electron transfer as well as being able to identify and order the important CT states between the chromophores. Furthermore, if these initial studies prove encouraging we would feel confident that we could use this method to systematically calculate excited state properties at various geometries. In this fashion we could study the interaction of CT states with low lying UV/vis excited states.

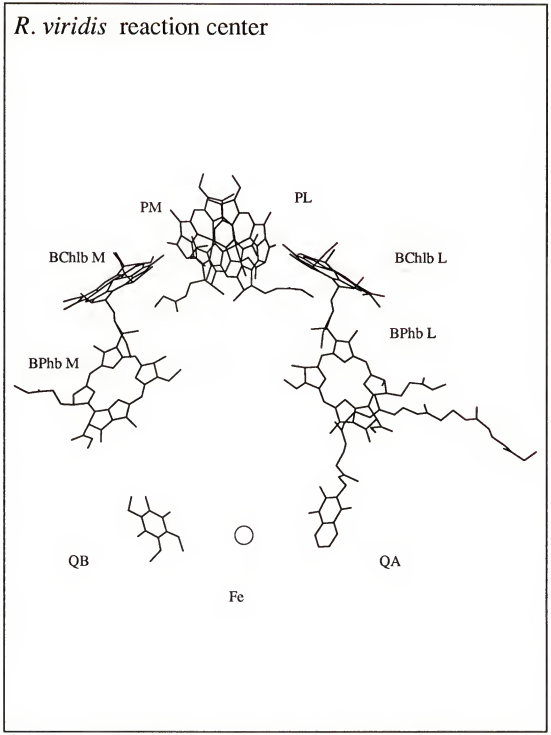

Figure 6.17 The chromophores of the photosynthetic reaction center of *Rps. viridis*[9].Abbreviations are: P_M, P_L = M and L BChlb of the special pair, $BChlb_M$, $BChlb_L$ = M and L auxiliary BChlb, $BPhb_M$, $BPhb_L$ = M and L BPhb, Q_A = quinone A (menaquinone), Q_B = quinone (ubiquinone), Fe = nonheme iron atom. This figure is positioned with the periplasmic (extracellular) side at the top and the cytoplasmic (intracellular) side at the bottom.

Our initial model of the RC consisted of the four BChlb and two BPhb chromophores (Figure 6.17). The phytol tails of these six molecules were truncated as in Figure 6.17. Also included were the four histidine amino acid side chains that coordinate with the fifth position of the Mg atoms of the BChlbs. This RC model contains 536 atoms, 1436 basis functions (minimal valence basis) and 1532 electrons. Furthermore, to obtain a reasonable description of the excited states using a single-excitation configuration interaction (CI) method requires the inclusion of a large number of configurations. To describe the low energy excited states just qualitatively correctly would require at least 144 configurations, which assumes each chromophore contributes the four orbitals of Gouterman's model[46]. We find in fact, that larger calculations are required for desired accuracy.

Results and Discussion

From the SCF, the MOs were found to be highly localized on the chromophores. The MOs of the BChlb dimer were localized to the dimer and demonstrate the supermolecule nature of the dimer. The percent localization of the 12 HOMOs and 12 LUMOs are shown in Table 6.30. Not shown in Table 6.30 are MOs 776 and 780 which were localized on the histidine rings coordinated with the auxiliary $BChlb_M$ and $BChlb_L$ respectively. The Mg-N(hist) distance for these two structure is 2.09 Å and 2.17 Å respectively. While the presence of these two MOs was somewhat surprising, we observe that single excited configurations involving MOs 776 and 780 did not contribute significantly to the low lying excited states of the RC model. Note also, in particular, that the highest lying occupied orbital is localized on the special pair. The lowest unoccupied orbital is localized on $BPhb_L$. This order of molecular orbitals by itself suggests flow of charge upon excitation in the observed direction along the L branch.

Table 6.30 Percent localization of the MOs for SCF of the RC model. The contribution from the histidine side chains are not shown.

MO	Energy a.u.	LP[a]	MP[b]	$BChlb_M$	$BChlb_L$	$BPhb_M$	$BPhb_L$
755	-0.268632						100
756	-0.265058					100	
757	-0.259928				99		
758	-0.259362			99			
759	-0.252014	38	61				
760	-0.237483	60	39				
761	-0.225687						100
762	-0.223854					100	
763	-0.213949				100		
764	-0.210893	4	4	92			
765	-0.210077	54	38	8			
766 (HOMO)	-0.204520	42	58				
767 (LUMO)	-0.080948						100
768	-0.075777					100	
769	-0.074284	61	39				
770	-0.069701				100		
771	-0.066951			100			
772	-0.055336	39	61				
773	-0.035711						100
774	-0.031468					100	
777	-0.010372				96		
778	-0.007819			85			
781	-0.003308	70	29				
782	-0.000816	29	70				

a: The L-BChlb of the dimer.
b: The M-BChlb of the dimer.

To see if we can relate the MOs of the RC model to specific MOs of the constituent chromophores calculated separately, we expand the RC MOs in a basis consisting of the MOs of the monomers and BChlb dimer, P.

$$\psi_i^{RC} = \sum_{\mu} |\varphi_\mu\rangle \langle\varphi_\mu|\psi_i^{RC}\rangle \tag{6.1}$$

Here the summation is over all the MOs of P, $BChlb_M$, $BChlb_L$, $BPhb_M$, and $BPhb_L$ where the coefficient that each basis MO contributes, $\langle\varphi_\mu|\psi_i^{RC}\rangle$, is the overlap of that MO with the RC MO. The MOs of the RC calculation were decomposed in this fashion using all MOs of the RCs constituents as a basis. The results are given in Table 6.31 where we show the contribution of the basis MOs that make up the 4–orbital model of Gouterman [46] for $BChlb_M$, $BChlb_L$, $BPhb_M$, and $BPhb_L$, and the 8–orbital model for the BChlb dimer, P, described previously (Chapter 4 and [90]). In this Table, orbitals labelled "d" are

$$\begin{aligned}
d_1, d_2 &= C_{11}\, a_{2u(L)} \pm C_{12}\, a_{2u(M)} \\
d_3, d_4 &= C_{21}\, a_{1u(L)} \pm C_{22}\, a_{1u(M)} \\
d_5, d_6 &= C_{31}\, e_{gx(L)} \pm C_{32}\, e_{gx(M)} \\
d_7, d_8 &= C_{41}\, e_{gy(L)} \pm C_{42}\, e_{gy(M)}
\end{aligned} \tag{6.2.2}$$

Where the coefficients C_{ij} depend on the specific configuration of the dimer. For example, we saw in Chapter 4 that these coefficients would correspond to $\frac{1}{\sqrt{2}}$ for the 5.0 Å separated Mg-bacteriochlorin dimer. In the above, D4h labels have been used to relate to the usual porphyrin-like electronic structure even though these molecules possess no particular symmetry. The RC MOs we show are those that dominate the low energy calculated spectra of the RC model and, as well, are described by the 4– and 8–orbital models.

Table 6.31 Coefficients for the 4–orbital and 8–orbital decomposition of selected RC MOs.

MO	P	$BChlb_M$	$BChlb_L$	$BPhb_M$	$BPhb_L$
755					0.999 a_{2u} [a]
756				0.999 a_{2u}	
757			0.966 a_{2u}		
758		0.963 a_{2u}			
759	0.966 d_1				
760	-0.976 d_2				
761					0.999 a_{1u}
762				0.999 a_{1u}	
763			-0.997 a_{1u}		
764		0.960 a_{1u}			
765	-0.958 d_3				
766	0.997 d_4				
(HOMO)					
767					0.999 e_{gx}
(LUMO)					
768				0.999 e_{gx}	
769	-0.997 d_5				
770			-0.998 e_{gx}		
771		0.998 e_{gx}			
772	-0.997 d_6				
773					0.999 e_{gy}
774				0.999 e_{gy}	
777			0.970 e_{gy}		
778		0.900 e_{gy}			
781	0.996 d_7				
782	0.989 d_8				

a The symmetry labels for the monomer MOs are from Gouterman. Although D4h symmetry labels do not strictly apply to reduced chlorins and their derivatives, the D4h symmetry labels are retained for convenience. The labels for the P MOs are from Figure 4.9.

A single excitation CI was performed to obtain a description of the UV/vis spectra of the RC model. The MO active space was chosen so as to balance the number of MOs on symmetry related chromophores on both the L and M branch (Figure 6.17). Thus the CI included all single excited configurations from the 40 highest occupied MOs into the 42 lowest virtual MOs. Including the ground state determinant, this resulted in 1681 configurations. The state and transition dipole moments included all one-center terms but omitted two-center terms. The calculated UV/vis spectrum for energies up to 22000 cm^{-1} is shown in Figure 6.18. We give a description of select CI states in Tables 6.32 – 6.34.

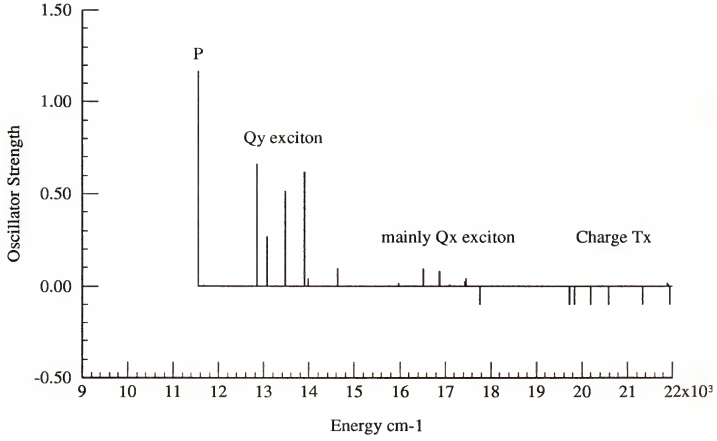

Figure 6.18 INDO/S calculated UV/vis spectra of the RC from *Rps. viridis.* The calculation includes 1681 singly excited configurations. The negative tics represent transitions with zero calculated oscillator strength.

Table 6.32 INDO/S UV/Vis Excited States for RC Model for up to 15000 cm^{-1}

State	Energy cm^{-1}	Oscillator Str.	Description
1	11550.1	1.1702	P : Qy1
2	12848.6	0.6646	P : Qy2 (mainly)
3	13069.2	0.2705	
4	13472.8	0.5168	Mixed Qy Exciton States
5	13898.1	0.6204	Of All 6 Chromophores
6	13981.1	0.0414	
7	14628.1	0.0966	P

Table 6.33 INDO/S UV/Vis Excited States for RC Model for States from 15000 cm^{-1} to 18000 cm^{-1}

State	Energy cm^{-1}	Oscillator Str.	Description
8	15976.0	0.0163	
9	16518.4	0.0950	mainly P
10	16877.3	0.0821	
11	17099.1	0.0073	$BPhb_L$: Qx
12	17305.6	0.0001	$BChlb_L$ -> $BPhb_L$: CT
13	17435.1	0.0259	$BPhb_M$, $BChlb_M$: Qx
14	17459.6	0.0121	$BChlb_M$, $BPhb_M$: Qx
15	17460.9	0.0421	$BChlb_L$: Qx
16	17765.4	0.0000	$BChlb_M$ -> $BPhb_M$: CT P -> $BChlb_M$: CT (small)
17	17809.4	0.0003	$BChlb_M$-> P : CT
18	17843.3	0.0001	$BChlb_L$ -> P : CT

Table 6.34 INDO/S UV/Vis Excited States for RC Model for States from 19000 cm^{-1} to 22000 cm^{-1}

State	Energy cm^{-1}	Oscillator Str.	Description
19	19728.4	0.0000	P -> $BPhb_L$: CT
20	19836.9	0.0000	P -> $BChlb_L$: CT
21	20192.5	0.0000	P -> $BChlb_M$: CT
22	20588.6	0.0000	P -> $BPhb_M$: CT

The two lowest energy transitions, states 1 and 2, correspond to the states Qy1 and Qy2 respectively (Chapters 4 and 5) based on the phase and magnitude of their major contributing configurations and the description of the MOs given in Table 6.31. These two states would correspond to the $P_{(-)}$ and $P_{(+)}$ lower and upper exciton components, respectively, of the BChlb dimer identified experimentally[92]. There has been some discussion in the literature concerning the placement of the upper exciton component of P. Experimentally, a shoulder located at 850 nm (11765 cm^{-1}) which is on the low energy side of the more intense absorption of the Qy bands of $BChlb_L$ and $BChlb_M$ is observed[92]. In their coupled chromophore treatment of the RC, Parson and Warshel attribute this shoulder to $BChlb_L$ and $BChlb_M$ and place the $P_{(+)}$ band at 812 nm with significant mixing with the Qy states of the other four chromophores in the RC[78]. Inasmuch as it is the second lowest excited in our calculation and it is the calculated upper exciton component of P (Chapters 4 and 5) our results are consistent with the identity of the upper exciton component with the shoulder at 850 nm

We define a pseudo C2 symmetry axis for this RC model that extends from the Fe atom to the average of the Mg atoms of P. The angle of the transition moments for the excited states with this axis can be compared to linear dichroism (LD) results[92]. We calculate this angle for Qy1 and Qy2 as 86.3° and 10.1° respectively. This compares to the corresponding experimental LD values given by Breton as 90° and 30° for $P_{(-)}$ and $P_{(+)}$ respectively[92]. We note here that there is some uncertainty in the value of 30°

for $P_{(+)}$ given by Breton. Calculations assuming only exciton coupling within the BChlb monomers of P give values of 88° and 10° for $P_{(-)}$ and $P_{(+)}$ respectively[92]. We calculate a splitting between Qy1 and Qy2 as 1299 cm^{-1} This is compared to previously calculated value of 1509 cm^{-1} for the "naked" BChlb dimer (Chapter 5) and to the experimental splitting of about 1350 cm^{-1} – 1700 cm^{-1} depending upon temperature[97, 92]. The CI used in the calculation of the RC model contained 17 occupied and 10 virtual MOs localized on the BChlb dimer. This amounts to 170 configurations specific to the active space of P. We do not span as large an active space for P in these RC calculations as we did in the calculations done previously on the naked BChlb (Chapter 5) . Thus we observe that the calculated energies of Qy1 and Qy2 for the RC model (11550.1 cm^{-1} and 12848.6 cm^{-1} respectively) are blue shifted compared to their calculated transition energies given previously (10982 cm^{-1} and 12490 cm^{-1} respectively). This represents a blue shift of 568 cm^{-1} and 359 cm^{-1} for Qy1 and Qy2 respectively. Furthermore, the splitting between these two bands has decreased from 1509 cm^{-1} for the dimer alone to 1299 cm^{-1} in the RC model. This smaller splitting is attributed to the increased mixing of Qy2 with the Qy bands from the other BChl and BPh monomers in the RC model which tends to retard the blue shift of Qy2 in this RC model. Thus we observe that Qy2 contains about 30–40% contributions from the Qy transitions from the two auxiliary BChlb and two BPhb chromophores (data not shown). A larger active space in the CI should red shift states Qy1 and Qy2 and may lessen the Qy contributions to Qy2 from the other chromophores in the RC.

To the high energy side of Qy2 are four states ranging in energy from 13069 cm^{-1} – 13981 cm^{-1} (765 nm – 715 nm). These states are dominated by Qy transitions from the four monomeric chromophores in the RC model with some small contribution from the Qy transitions from P. These states do not exhibit any largely dominant Qy transition from the monomer chromophores, and further labelling of them here is inappropriate. We merely observe that, in accord with experiment, we calculate the Qy exciton states

of the branch chromophores just to the high energy side of Qy2. Our INDO/S method is parametrized to reproduce low energy UV/vis spectra of molecules like benzene and pyridine[38]. This parameterization is based on a singles only configuration interaction. It is commonly observed that CI-singles methods systematically overestimate transition probabilities. Inclusion of certain low lying double excitations to the CI do in fact give more reasonable oscillator strengths. Thus we expect that our INDO/S calculations may overestimate the exciton coupling interactions between the auxiliary BChlbs and the BPhbs in our RC model. We observe that these four Qy based states show significant mixing between the Qy transitions of $BChlb_L$, $BChlb_M$, $BPhb_L$, and $BPhb_M$ making it difficult to assign them to specific chromophores as can be done experimentally. From LD experiments, the angle between the RC C2 axis and the Qy transitions for $BChlb_M$, $BChlb_L$, $BPhb_M$, and $BPhb_L$ have been determined to be roughly 70°, 70°, 40°, and 40° respectively[92]. The calculated angles for states 3–6 from Table 6.32 are 67°, 52°, 66°, and 73°, respectively. The experimental values bracket our values and appear to reflect an averaging of the branch chromophores Qy angles consistent with the strong mixing we observe in our calculations.

Several states are dominated by transitions between chromophores and are labelled as CT states. The energies and difference in state dipole moments for these states with the ground state are given in Table 6.35. We have found that these states are usually dominated by one or two configurations representing interchromophore excitations. As such we observe that the placement of these CT transitions in our calculations is largely insensitive to the size of the active space in the CI. The energies of these CT states can be estimated from the SCF results and knowledge of the RC geometry by the formula

$$E_{CT} \approx \epsilon^{A}_{occ} - \epsilon^{B}_{virt} - \frac{1}{R_{ab}} \tag{6.2.3}$$

which is merely the difference in orbital energies on chromophores A and B offset by the coulomb interaction between the separated charge. We have ignored exchange which should be small for chromophores that are well separated. Thus we can estimate the E_{CT}

for P->$BPhb_L$ based on the energies of the HOMO and LUMO from our RC calculation (Table 6.30) and the center to center distance of about 17 Å between P and $BPhb_L$. We obtain a value of about 20290 cm^{-1} compared to 19728 from our CI calculation (Table 6.34).

Table 6.35 Calculated energies and dipole moment differences with the ground state for selected CT states from the RC model.

State[a]	Energy cm^{-1}	$\Delta\mu_x$ [b]	$\Delta\mu_y$	$\Delta\mu_z$	$\lvert\Delta\mu\rvert$	Description
12	17305.6	-9.91	-41.69	21.93	48.14	$BChlb_L$ -> $BPhb_L$
16	17765.4	-38.77	-24.50	14.32	48.05	$BChlb_M$ -> $BPhb_M$
17	17809.4	27.58	-21.99	-28.34	45.25	$BChlb_M$ -> P
18	17843.3	-10.98	34.00	20.92	41.40	$BChlb_L$ -> P
19	19728.4	-12.30	-77.92	-2.01	78.90	P -> $BPhb_L$
20	19836.9	0.46	-48.69	10.82	49.88	P -> $BChlb_L$
21	20192.5	-23.85	14.39	48.02	55.51	P -> $BChlb_M$
22	20588.6	-51.64	-15.19	54.95	76.92	P -> $BPhb_M$

a: number of states is the same as in Tables 6.33 and 6.34
b: The calculated dipole moment of the excited state – ground state (units are Debyes).

The large values of $|\Delta\mu|$ and their vectorial direction are consistent with the CT character of these states between the relevant chromophores. Note that states P–>$BPhb_L$ and P–>$BPhb_M$ have the largest values of $|\Delta\mu|$, being 78.9 and 76.92 Debye respectively. These dipole magnitudes are roughly 1.5–2.0 times as large as the other CT states which is indicative of the larger distance involved in the charge separation relative to the other states. The asymmetry of the RC model is apparent in the relative ordering of analogous CT states involving the L and M branch chromophores. Charge transfer from P to the BChlb and BPhb energetically favors the L vs. the M branch by 860 cm^{-1} and 356 cm^{-1} (states 19,22 and 20,21). As well, CT states from the corresponding BChlb to BPhb for the L vs. the M arm favors the L arm by 460 cm^{-1} (states 12,16).

For these gas phase calculations, the energy separation between Qy1 and the CT states ranges from about 6000–9000 cm^{-1}. We would expect, for a pseudoactivationless primary electron transfer[29], that the relevant CT states would be accessible to the lowest excited state by a much smaller energy gap than is demonstrated by our calculation. The expected energy gap would be on the order of a vibrational energy (about 1000–2000 cm^{-1}). Also, these results give $BChlb_L$ –> $BPhb_L$ as the lowest accessible CT state, being almost 2400 cm^{-1} lower in energy than P->$BChlb_L$ and P->$BPhb_L$. Even assuming that the energies if these CT states are strongly affected by small geometric changes, it is difficult to envision that these changes would reorder the CT states and place them energetically close to Qy1.

The chromophores of the RC are imbedded within a membrane protein complex. There are several nearby amino acids that exhibit specific interactions with the chromophores which may effect the photophysical and dynamic properties of the RC. However the remainder of the surrounding protein can also act as a polarizable solvent. Due to the large change in dipole moment of the CT states, we should address the effects of a polarizable solvent medium on the energy and ordering of these states. We include the effects of a solvent using the self-consistent reaction field method of Tapia & Goscinski[99] and Karelson & Zerner[100]. This model treats the solvent as an isotropic polarizable medium. The solvation effect is treated as a perturbation, H_1, to the Hamiltonian of the isolated molecule, H_o.

$$H_{rf} = H_o + H_1 \tag{6.2.4}$$

A set of modified Fock equations that incorporates this solvent perturbation is derived.

$$\hat{f} = \hat{f_o} - g\,\hat{\mu} \cdot \langle \mu \rangle \tag{6.2.5}$$

$$g = \frac{1}{a_o^3}\left(\frac{\epsilon - 1}{2\epsilon + 1}\right) \tag{6.2.6}$$

Where ϵ is the solvent dielectric constant, $\hat{\mu}$ the dipole moment operator, and a_o the effective radius of the solvent cavity. The second term in eqn. 6.2.5 represents the reaction field at the solute molecule generated by the solvent which can change each SCF cycle in response to the dipole moment of the solute, $\langle\mu\rangle$. These Self Consistent Reaction Field (SCRF) equations are solved iteratively in the usual fashion until an SCF is achieved. A single excited CI is performed from the single determinant SCRF ground state. The energy correction to the excited states is given as

$$E_{corr} = -\frac{1}{a_o^3}\left(\frac{\eta^2-1}{2\eta^2+1}\right)(\langle\mu^*\rangle - \langle\mu\rangle)\cdot\langle\mu^*\rangle \qquad (6.2.7)$$

Where η represents the solvent refractive index and $\langle\mu^*\rangle$ the dipole moment of the solute excited state. The reaction field model assumes a spherical solvent cavity with radius a_o. Our choice of a value for a_o is based the mass density of the RC model we used for the calculations.

$$\frac{4}{3}\pi a_o^3 = \frac{M}{\rho} \qquad (6.2.8)$$

Where M is the molar mass and ρ is the mass density of the RC model. We used a value of 1.336 g/cm^3 for ρ which is the mass density of porphin. This formulation gave us an effective cavity radius of 10.6 Å. We modelled the protein as a solvent having the bulk properties of cyclohexane (ϵ = 2.023 and ρ = 1.4266).

The results of the calculated UV/vis spectra of our RC model employing the above solvent model showed relatively little change to the local exciton-like excited states. This is what we would expect for states exhibiting small dipole changes. The Qy1 state does exhibit some internal CT character between the BChlb monomers (Chapter 5) and we do observe small shift in energy from 11550 cm^{-1} to 11461 cm^{-1} in the gas phase and solvent calculations respectively. However, we observe relatively large changes in the energies and ordering of the calculated CT states. Table 6.36 and Figure 6.19 compare the results for the CT states in the gas phase and the solvent calculation. Note that the CT states are all lowered in energy and their relative ordering is changed. We calculate

that P->$BPhb_L$ is now within about 1200 cm^{-1} of Qy1. As well, CT from P to both the BPhb chromophores is lower in energy that from P to the auxiliary BChlb chromophores. This concurs with the lack of an experimentally observed intermediate involving wither $BChlb_L^+$ or $BChlb_L^-$ in picosecond and sub-picosecond experiment[21]. The splitting between P–>$BPhb_L$ and P->$BChlb_L$ is about 4000 cm^{-1} whereas the splitting between P–>$BPhb_L$ and $BChlb_L$–>$BPhb_L$ is about 1300 cm^{-1}. Our results suggest against an explicit intermediate involving $BChlb_L$[101].

Table 6.36 INDO/S calculated energies and dipole moment differences with the ground state for Qy1 and CT states from the RC model.

State	Gas Phase Calculation		Solvent Calculation[b]	
	Energy cm^{-1}	$\Delta\mu$[a]	Energy cm^{-1}	$\Delta\mu$
Qy1	11550.1	4.6	11460.6	4.6
B_L -> H_L	17305.6	48.1	13947.5	47.1
B_M -> H_M	17765.4	48.1	14405.7	47.1
P -> H_L	19728.4	78.9	12608.7	75.0
P -> B_L	19836.9	49.9	16597.9	46.1
P -> B_M	20192.5	55.5	16713.4	48.4
P -> H_M	20588.6	76.9	13496.3	74.8

a: The calculated dipole moment of the excited state – ground state (units are Debyes).

b: ϵ = 2.023, η = 1.4266, and a_o = 10.6 Å (see text)

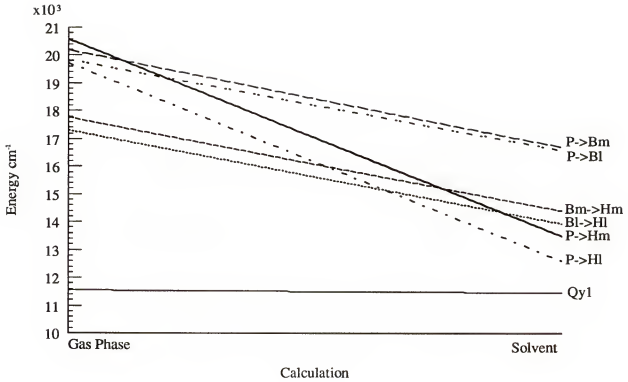

Figure 6.19 Energies of CT states and Qy1 in the absence and presence of solvent.

The states representing the lowest excited state of the RC and the initial CT event are connected dynamically. We do not specifically address any dynamic aspects of the RC in our calculations. Furthermore, there are surely dynamic effects due to explicit protein residues and the phytol tails of the chromophores, as well as the other chromophores present in the RC (Figure 6.17). Our solvent model is somewhat crude. It assumes a spherical cavity within an isotropic dielectric medium. While the effects of the solvent model on the SCF are of high order (the solute is allowed to relax in the presence of the reaction field) the corrections to the excited state for electronic reorganization are limited to first order. Thus we probably overemphasize the solvent effect in the absorption spectrum. Furthermore, there will be some reorientational relaxation of the

solvent during the lifetime of the excited state, and this has not been accounted for. Yet we have demonstrated that in both the gas phase and solvent calculation that the asymmetry between the L and M branch is evident and favors transitions involving the L branch which is consistent with experiment. Also we observe that the CT transition representing the product of the primary CT event is within typical vibrational energies of the lowest excited state Qy1. We conclude by noting that these results do indicate that consideration of the protein as a polarizable solvent is important to the energies and relative ordering of the CT states, and explain transfer along the L branch as well as supplying a rationale for the absence of an active participation of the auxiliary BChl.

CHAPTER 7
CONCLUSIONS

The theoretical study of the photosynthetic reaction center (RC) is a large undertaking. While there are certainly limitations to what we can address in a system this large and complex, there are many aspects of this system that can be effectively examined using theory. When the X-ray structure of the RC was first published we necessarily began by examining small pieces of it in order to establish the effectiveness of our methods as well as to gain an understanding of some simpler aspects before attempting to study models of all the pigments together. When I first began this work, spectroscopic calculations on dimers of bacteriochlorophyll were not routinely done, not to mention all six pigments of the RC. Instead, simple coupled chromophore models were the mainstay of research in this area for many years, in part, because they could recast a large complex problem in terms of a small number of interactions making the calculations feasible on small computers. The limitations of these phenomenological models made them inadequate for understanding some important properties of RCs most notably the supermolecule nature of the BChlb dimer. I chose to use less arbitrary, albeit semi-empirical, methods to examine the electronic structure and properties of the RC and its pigments. This approach has prooven successful and I feel the results outlined in this dissertation have contributed to a better understanding of the properties of these interesting systems.

In Chapter 2 we demonstrated that nearby charged or polar groups have noticeable effects on the calculated properties of chlorophylls and related molecules. These effects display distinct patterns as to charge and placement around the macrocycle ring and are readily understood in terms of simple point charge-dipole interactions that differ for the

ground and excited states leading to shifts in the calculated UV/vis transitions. These results were extended to examine the electrochromic effects of the initial photosynthetic electron transfer products, $(P^+)(BChlb_L)(BPhb_L^-)$ on the Qy absorption of the bridging $BChlb_L$ in the RC. In picosecond experiments, a transient diminishing of the intensity of the Qy band of the auxiliary BChl ($BChlb_L$) was observed. This initially led to some speculation about a possible role for $BChlb_L$ as an explicit intermediate in the CT reaction. We calculate blue shifts in the Qy band of $BChlb_L$ due to the presence of P^+ and $BPhb_L^-$ which would negate this shift as evidence for a role of $BChlb_L$ as an explicit intermediate on picosecond timescale. Rather, our results indicate that this spectroscopic evidence can be explained as a transient blue shift induced by a Stark effect and not necessarily a bleaching of this band through reduction. Recently, subpicosecond experiments have also argued against an explicit intermediate involving $BChlb_L$ in the initial photochemical event.[21].

Perhaps one of the more controversial aspects of the properties of the RC in the past had been the causes for the anomalous red shift observed from *in vitro* to *in vivo* for the Q bands of BChls. Many causes were invoked such as nearby charged groups, large solvent effects, and aggregation of BChls. When the X-ray crystal structure of the RC was first published it was seen that there was a dimer of BChl molecules. However existing coupled chromophore models could still not explain the anomalous red shift, even given the specific geometry. Unknown 'protein effects' were still invoked in these models to get reasonable agreement with experiment. We demonstrate that the BChl dimer is not explained well by a simple coupled chromophore model and we argue for a supermolecule description that better explains the UV/vis features of the BChl dimer[67], Chapter 3. While these arguments are simple they have profound implications. The RC must contain the UV/vis excitation of lowest energy for it to act effectively as a phototrap. Thus an understanding of this red shift is crucial to understanding the initiation of the photochemistry of RCs.

In Chapter 4 we show, using dimers of Mg-bacteriochlorin, that CT excitation between the monomers must be considered to understand the low energy Qy band of these dimers. These model studies were extended in Chapter 5 to the real BChl dimer and demonstrated the importance of these intra-dimer CT transitions. We also examined the effects of some of the nearby amino acids on the BChl dimer and observe that small changes in the placement of the protons involved in H-bonding can have large changes on the calculated UV/vis spectrum of the BChl dimer.

In Chapter 6 we performed quantum chemical calculations on a RC model. Our results are consistent with the lowest energy electronic transition and the shoulder at 850 nm in the experimental spectrum being the lower and upper exciton-like components of the Qy transitions of the BChl dimer respectively. We calculate the presence of bands consisting of the Qy transitions of the remaining chromophores of the RC just to the high energy side of the two BChl dimer bands. Though these Qy bands have the correct placement relative to the two BChl dimer absorptions, they exhibit no obvious monomer parentage as can be discerned experimentally. The overestimate of exciton coupling between the auxiliary BChlbs and the BPhbs was discussed as one reason for this observation. We find several CT states about 6000–9000 cm^{-1} higher in energy than the lowest excited state of the RC model. These CT states show that the L branch of the RC is favored over the M branch. Though these results do not address any dynamics that surely connect the lowest excited state and the CT states, the relative ordering of our calculated CT states is consistent with the experimental observation of appreciable CT along only the L branch. These initial calculations of the RC represent gas phase calculations, that is to say, we neglect any protein effects. By applying a simple solvent model that treats the protein as a polarizable medium we find that the CT states have all dropped considerable in energy with some reordering relative to the gas phase calculation. The CT state that is most accessible to the lowest excited state of the RC is now the P->$BPhb_L$ which is consistent with experimental observation. This CT state is within about 1200 cm^{-1} of

the lowest excited state and this energy spacing seems much more reasonable in terms of this CT state being vibrationally accessible to the lowest excited state. These results are also consistent with the lack of any observable intermediate involving the auxiliary BChls. The solvent calculation still maintains the energetic preference for the L branch in terms of corresponding CT states involving chromophores related by the pseudo C2 symmetry axis of the RC. While certainly simple, these solvent calculations demonstrate that the protein modelled as a polarizable medium may be important to the energy and relative ordering of the CT states of the RC.

This work outlined in this dissertation has attempted to answer many questions. In addition it has generated many more questions that require attention. One exciting piece of work that could follow from this dissertation would be to calculate the UV/vis excited states (specifically the CT states) of a RC model along some geometric coordinate that ideally represents the trajectory for electron transfer. This coordinate is certainly complex involving some 3N coordinates where N represents at least the number of chromophore atoms and many nearby amino acid residues. Identifying this coordinate represents a significant challenge. Currently only methods based on classical force fields have been applied to systems of this size. Of course these classical force fields are parameterized on experiment and may not give reasonable representations for BChls. However the goal of this work would be to merely attempt a reasonable description of the essential physics of the process. Therefore a 'reasonable' trajectory could very possibly be identified.

BIBLIOGRAPHY

[1] R. K. Clayton, Photosynthesis: physical mechanisms and chemical patterns, volume 4 of IUPAB Biophysics Series, chapter 1, 9, pages 1–19, 191–226, Cambridge University Press, Cambridge, 1980.

[2] M. Wilson, Lives in Science, A Scientific American Book, Simon and Schuster, New York, 1957.

[3] W. D. Edwards and M. C. Zerner, Int. J. Quantum Chem. **23**, 1407 (1983).

[4] P. J. Kiley and S. Kaplan, Microbiological Reviews **52**, 50 (1988).

[5] A. L. Lehninger, Biochemistry, chapter 22, 23, pages 587–615, 623–657, Worth Publishers, Inc., New York, 2 edition, 1975.

[6] I. Witt et al., Ber. Bunsenges. Phys. Chem. **92**, 1503 (1988).

[7] J. Deisenhofer, O. Epp, K. Miki, R. Huber, and H. Michel, J. Mol. Biol. **180**, 385 (1984).

[8] J. Deisenhofer, O. Epp, K. Miki, R. Huber, and H. Michel, Nature **318**, 618 (1985).

[9] J. Deisenhofer and H. Michel, The crystal structure of the photosynthetic reaction center from rhodopseudomonas viridis, in The Photosynthetic Bacterial Reaction Center Structure and Dynamics, edited by J. Breton and A. Vermeglio, pages 1–3, New York, 1988, NATO ASI Series, Plenum Press.

[10] T. O. Yeates et al., Proc. Natl. Acad. Sci. USA **85**, 7993 (1988).

[11] E. C. Kellogg, S. Kolaczkowski, M. R. Wasielewski, and D. M. Tiede, Photosynthesis Research **22**, 47 (1989).

[12] G. Feher, J. P. Allen, M. Y. Okamura, and D. C. Rees, Nature **339**, 111 (1989).

[13] C. Kirmaier and D. Holten, Photosynthesis Research **13**, 225 (1987).

[14] L. K. Hanson, Photochemistry and Photobiology **47**, 903 (1988).

[15] R. E. Blankenship and W. W. Parson, Biochimica et Biophysica Acta **545**, 429 (1979).

[16] R. J. Debus, G. Feher, and M. Y. Okamura, Biochemistry **25**, 2276 (1986).

[17] J. R. Norris, R. A. Uphaus, H. L. Crespi, and J. J. Katz, Proc. Natl. Acad. Sci. USA **68**, 625 (1971).

[18] J. R. Norris, H. Scheer, M. E. Druyan, and J. J. Katz, Proc. Natl. Acad. Sci. USA **71**, 4897 (1974).

[19] J. Fajer, D. C. Brune, M. S. Davis, A. Forman, and L. D. Spaulding, Proc. Natl. Acad. Sci. USA **72**, 4956 (1975).

[20] J. Jortner, J. Am. Chem. Soc. **102**, 6676 (1980).

[21] G. R. Fleming, J. L. Martin, and J. Breton, Nature **133**, 190 (1988).

[22] J. Breton, J. L. Martin, J. Petrich, A. Migus, and A. Antonetti, FEBS Letters **209**, 37 (1986).

[23] L. Martin, J. Breton, A. J. Hoff, A. Migus, and A. Antonetti, Proc. Natl. Acad. Sci. USA **83**, 957 (1986).

[24] R. A. Marcus and N. Sutin, Biochimica et Biophysica Acta **811**, 265 (1985).

[25] N. W. Woodbury and W. W. Parson, Biochimica et Biophysica Acta **850**, 197 (1986).

[26] R. A. Friesner and Y. Won, Biochimica et Biophysica Acta **977**, 99 (1989).

[27] A. Warshel, Proc. Natl. Acad. Sci. USA **77**, 3105 (1980).

[28] R. A. Marcus, Chem. Phys. Letts. **133**, 471 (1987).

[29] M. Bixon and J. Jortner, Chem. Phys. Letts. **159**, 17 (1989).

[30] M. Bixon, J. Jortner, M. Plato, and M. E. Michel-Beyerle, Mechanism of the primary charge separation in bacterial photosynthetic reaction centers, in The Photosynthetic Bacterial Reaction Center Structure and Dynamics, edited by J. Breton and A. Vermeglio, pages 399–419, New York, 1988, NATO ASI Series, Plenum.

[31] M. Plato, K. Mobius, M. E. Michel-Beyerle, M. Bixon, and J. Jortner, J. Am. Chem. Soc. **110**, 7279 (1988).

[32] M. Bixon, M. E. Michel-Beyerle, and J. Jortner, Israel J. Chem. **28**, 155 (1988).

[33] P. O. J. Scherer and F. Fischer, Chem. Phys. **131**, 115 (1989).

[34] R. A. Marcus, Early steps in bacterial photosynthesis. comparison of three mechanisms, in The Photosynthetic Bacterial Reaction Center Structure and Dynamics, edited by J. Breton and A. Vermeglio, pages 389–398, New York, 1988, NATO ASI Series, Plenum.

[35] L. K. Hanson, J. Fajer, M. A. Thompson, and M. C. Zerner, J. Am. Chem. Soc. **109**, 4728 (1987).

[36] L. K. Hanson, M. A. Thompson, and J. Fajer, Environmental effects on the properties of chlorophylls in vivo. theoretical models, in Progress in Photosynthetic Research, edited by B. J., pages 311–314, New York, 1987, Martinus Nijhoff.

[37] L. K. Hanson, M. A. Thompson, M. C. Zerner, and J. Fajer, Theoretical models of electrochromic and environmental effects on bacterio-chlorophyll and -pheophytins in reaction centers, in The Photosynthetic Bacterial Reaction Center, edited by B. J. and V. A., pages 355–367, Plenum, 1988.

[38] J. Ridley and M. Zerner, Theoret. Chim. Acta **32**, 111 (1973).

[39] J. E. Ridley and M. C. Zerner, Theoret. Chim. Acta **42**, 223 (1976).

[40] M. C. Zerner, G. H. Loew, R. F. Kirchner, and U. T. Mueller-Westerhoff, J. Am. Chem. Soc. **102**, 589 (1980).

[41] J. A. Pople, D. P. Santry, and G. A. Segal, J. Chem. Phys. **43**, S129 (1965).

[42] J. A. Pople and G. A. Segal, J. Chem. Phys. **43**, S136 (1965).

[43] J. A. Pople and G. A. Segal, J. Chem. Phys. **44**, 3289 (1966).

[44] J. A. Pople, D. L. Beveridge, and P. A. Dobosh, J. Chem. Phys. **47**, 2026 (1967).

[45] H. Chow, R. Serlin, and C. E. Strouse, J. Am. Chem. Soc. **97**, 7230 (1975).

[46] M. Gouterman, J. Mol. Spec. **6**, 138 (1961).

[47] L. K. Hanson et al., J. Am. Chem. Soc. **106**, 3950 (1984).

[48] R. C. Davis, S. L. Ditson, A. F. Fentiman, and R. M. Pearlstein, J. Am. Chem. Soc. **103**, 6823 (1981).

[49] J. Eccles and B. Honig, Proc. Natl. Acad. Sci. USA **80**, 4959 (1983).

[50] J. Del Bene and H. H. Jaffe, J. Chem. Phys. **48**, 1807 (1968).

[51] J. Breton, J. L. Martin, A. Migus, A. Antonetti, and A. Orszag, Proc. Natl. Acad. Sci. USA **83**, 5121 (1986).

[52] C. Kirmaier, D. Holten, and W. W. Parson, Biochimica et Biophysica Acta **725**, 190 (1983).

[53] C. Kirmaier, D. Holten, and W. W. Parson, FEBS Letters **185**, 76 (1985).

[54] H. Michel, O. Epp, and J. Deisenhofer, EMBO **5**, 2445 (1986).

[55] C. H. Chang et al., FEBS Letters **205**, 82 (1986).

[56] J. P. Allen, G. Feher, T. O. Yeates, H. Komiya, and D. C. Rees, Proc. Natl. Acad. Sci. USA **84**, 5730 (1987).

[57] V. A. Shuvalov and L. N. M. Duysens, Proc. Natl. Acad. Sci. USA **83**, 1690 (1986).

[58] V. A. Shuvalov, J. Amez, and L. N. M. Diysens, Biochimica et Biophysica Acta **851**, 327 (1986).

[59] M. S. Davis, A. Forman, L. K. Hanson, J. P. Thornber, and J. Fajer, J. Phys. Chem. **83**, 3325 (1979).

[60] A. Vermeglio and R. K. Clayton, Biochimica et Biophysica Acta **461**, 159 (1977).

[61] P. Maroti, C. Kirmaier, C. Wraight, D. Holten, and R. M. Pearlstein, Biochimica et Biophysica Acta **810**, 133 (1985).

[62] M. R. Wasielewski, J. R. Norris, H. L. Crespi, and J. Harper, J. Am. Chem. Soc. **103**, 7664 (1981).

[63] M. R. Wasielewski, J. R. Norris, L. L. Shipman, C. Lin, and W. A. Svec, Proc. Natl. Acad. Sci. USA **78**, 2957 (1981).

[64] P. J. O'Malley and G. T. Babcock, Proc. Natl. Acad. Sci. USA **81**, 1098 (1984).

[65] B. Ward, C. K. Chang, and R. Young, J. Am. Chem. Soc. **106**, 3943 (1984).

[66] L. L. Maggiora, J. D. Petke, D. Gopal, R. T. Iwamoto, and G. M. Maggiora, Photochemistry and Photobiology **42**, 69 (1985).

[67] M. Thompson and M. Zerner, J. Am. Chem. Soc. **110**, 606 (1988).

[68] M. Plato, E. Trankle, W. Lubitz, F. Lendzian, and K. Mobius, Chem. Phys. **107**, 185 (1986).

[69] L. L. Shipman, J. R. Norris, and J. J. Katz, J. Phys. Chem. **80**, 877 (1976).

[70] A. Warshel, J. Am. Chem. Soc. **101**, 744 (1979).

[71] J. D. Petke and G. M. Maggiora, J. Chem. Phys. **84**, 1640 (1986).

[72] D. E. LaLonde, J. D. Petke, and G. M. Maggiora, J. Phys. Chem. **93**, 608 (1989).

[73] P. O. J. Scherer and S. F. Fischer, Chem. Phys. Letts. **131**, 153 (1986).

[74] E. W. Knapp et al., Proc. Natl. Acad. Sci. USA **82**, 8463 (1985).

[75] A. Scherz and W. W. Parson, Biochimica et Biophysica Acta **766**, 666 (1984).

[76] R. M. Pearlstein, Chlorophyll singlet excitons, in Photosynthesis, edited by Govindjee, pages 294–330, New York, 1982, Academic Press.

[77] A. Warshel and W. W. Parson, J. Am. Chem. Soc. **109**, 6143 (1987).

[78] W. W. Parson and A. Warshel, J. Am. Chem. Soc. **109**, 6152 (1987).

[79] J. Eccles, B. Honig, and K. Schulten, Biophys. J. **53**, 137 (1988).

[80] E. W. Knapp, P. O. J. Scherer, and S. F. Fischer, Biochimica et Biophysica Acta **852**, 295 (1986).

[81] T. Azumi and S. P. McGlynn, J. Chem. Phys. **41**, 3131 (1964).

[82] T. Azumi, A. Armstrong, and T. McGlynn, J. Chem. Phys. **41**, 3839 (1964).

[83] M. Losche, G. Feher, and M. Y. Okamura, The stark effect in photosynthetic reaction centers from rhodobacter sphaeroides r-26, rhodopseudomonas viridis and the d1d2 complex of photosystem ii from spinach, in The Photosynthetic Bacterial Reaction Center Structure and Dynamics, edited by J. Breton and A. Vermeglio, pages 151–164, New York, 1988, NATO ASI Series, Plenum Press.

[84] M. Plato, F. Lendzian, W. Lubitz, E. Trankle, and K. Mobius, Molecular orbital studies on the primary donor p960 in reaction centers of rps. viridis, in The Photosynthetic Bacterial Reaction Center Structure and Dynamics, edited by J. Breton and A. Vermeglio, pages 379–388, New York, 1988, NATO ASI Series, Plenum Press.

[85] K. M. Barkigia, L. Chantranupong, K. M. Smith, and J. Fajer, J. Am. Chem. Soc. **110**, 7566 (1988).

[86] D. J. Lockhart and S. G. Boxer, Proc. Natl. Acad. Sci. USA **85**, 107 (1988).

[87] H. P. Braun, M. E. Michel-Beyerle, J. Breton, S. Buchanan, and H. Michel, FEBS Letters **221**, 221 (1987).

[88] M. Losche, G. Feher, and M. Y. Okamura, Proc. Natl. Acad. Sci. USA **84**, 7537 (1987).

[89] M. Thompson and M. Zerner, Calculations on the spectroscopy of large molecular systems: An examination of the spectroscopy of model chlorophyll dimers, in Photosynthesis and Electron-Transport, edited by P. Poncascau and L. Skala, Prague, Czechoslovakia, 1990, Charles University Press, in press.

[90] M. Thompson and M. Zerner, J. Phys. Chem. (1990), accepted.

[91] J. D. Petke, G. M. Maggiora, L. L. Shipman, and R. E. Christoffersen, Photochemistry and Photobiology **30**, 203 (1979).

[92] J. Breton, Biochimica et Biophysica Acta **810**, 235 (1985).

[93] D. M. Tiede et al., Symmetry breaking structures involved in the docking of cytochrome c and primary electron transfer in reaction centers of rhodobacter sphaeroides, in The Photosynthetic Bacterial Reaction Center Structure and Dynamics, edited by J. Breton and A. Vermeglio, pages 13–20, New York, 1988, NATO ASI Series, Plenum Press.

[94] E. J. Bylina, C. Kirmaier, L. McDowell, D. Holten, and D. C. Youvan, Nature **336**, 182 (1988).

[95] M. Plato, W. Lubitz, and F. Lendzian, Israel J. Chem. **28**, 109 (1988).

[96] W. L. Reynolds and R. W. Lumry, Mechanisms of Electron Transfer, page 91, The Ronald Press Company, New York, 1966.

[97] A. Vermeglio and G. Paillotin, Biochimica et Biophysica Acta **681**, 32 (1982).

[98] C. Kirmaier and D. Holten, Temperature effects on the ground state absorption spectra and electron transfer kinetics of bacterial reaction centers, in The Photosynthetic Bacterial Reaction Center Structure and Dynamics, edited by J. Breton and A. Vermeglio, pages 219–228, New York, 1988, NATO ASI Series, Plenum Press.

[99] O. Tapia and O. Goscinski, Mol. Phys. **29**, 1653 (1975).

[100] M. Karelson and M. C. Zerner, 1990, In preparation.

[101] R. A. Marcus, Israel J. Chem. **28**, 205 (1988).

BIOGRAPHICAL SKETCH

I grew up in Richfield, Minnesota on the outskirts of Minneapolis. Before starting my undergraduate education I worked as a SCUBA instructor for four years and travelled in the Caribbean on numerous tours in connection with this job. I attended the University of Minnesota and received a B.S. in biology in 1983 after which I was employed as a chemist for 1 1/2 years working on the isolation and characterization of fungal enzymes. In 1985 I entered the department of Chemistry at the University of Florida to begin studies for my Ph.D.

I certify that I have read this study and that in my opinion it conforms to acceptable standards of scholarly presentation and is fully adequate, in scope and quality, as a dissertation for the degree of Doctor of Philosophy.

Michael Zerner
Professor of Chemistry

I certify that I have read this study and that in my opinion it conforms to acceptable standards of scholarly presentation and is fully adequate, in scope and quality, as a dissertation for the degree of Doctor of Philosophy.

Samuel Colgate
Associate Professor of Chemistry

I certify that I have read this study and that in my opinion it conforms to acceptable standards of scholarly presentation and is fully adequate, in scope and quality, as a dissertation for the degree of Doctor of Philosophy.

N. Yngve Öhrn
Professor of Physics

I certify that I have read this study and that in my opinion it conforms to acceptable standards of scholarly presentation and is fully adequate, in scope and quality, as a dissertation for the degree of Doctor of Philosophy.

John Sabin
Professor of Physics

I certify that I have read this study and that in my opinion it conforms to acceptable standards of scholarly presentation and is fully adequate, in scope and quality, as a dissertation for the degree of Doctor of Philosophy.

William Weltner
Professor of Chemistry

This dissertation was submitted to the Graduate Faculty of the Department of Chemistry in the College of Liberal Arts and Sciences and to the Graduate School and was accepted as partial fulfillment of the requirements for the degree of Doctor of Philosophy.

August 1990

Dean, Graduate School